UNIVERSITY OF OKLAHOMA

GRADUATE COLLEGE

TRANSIENT TEMPERATURE BEHAVIOR IN A WELLBORE AND SURROUNDING FORMATION

A THESIS

SUBMITTED TO THE GRADUATE FACULTY

in partial fulfillment of the requirements for the

Degree of

MASTER OF SCIENCE

By

YU JIANG
Norman, Oklahoma
2017

TRANSIENT TEMPERATURE BEHAVIOR IN A WELLBORE AND SURROUNDING FORMATION

A THESIS APPROVED FOR THE
MEWBOURNE SCHOOL OF PETROLEUM AND GEOLOGICAL ENGINEERING

BY

_____
Dr. Xingru Wu, Chair

_____
Dr. Siddharth Misra

_____
Dr. Ahmad Jamili

This work is dedicated to my family and my friends.

Acknowledgements

Firstly, I would like to express my sincere appreciation to my supervisor, Dr. Xingru Wu, for his guidance and kind help in both my research and my life during the past two years. I would never get the chance to make progresses without his encourage and help.

I would also like to give my thanks to Dr. Siddharth Misra and Dr. Ahmad Jamili, for their valuable comments and time spent serving as my thesis defense committee members.

I would like to give my thanks to Dr. Jianchun Xu and Mr. Wenchao Teng at China University of Petroleum, for their help and suggestions on my research work.

Finally, I would like to thank my family who are supporting me during my whole life, and my friends and many others who kindly gave their help to me.

Table of Contents

List of Tables

List of Figures

Abstract

Transient temperature behavior in a wellbore develops as a result of heat exchange between fluid in the wellbore and surrounding formation as the hot fluid from reservoir moves upward in production, or vice versa during injection. Previous models based upon steady-state mass flow rate or semi-steady state heat transfer cannot be applied for many practical scenarios such as variant production rates and deep water flow assurance management, to give accurate results which are critical in many decision-making situations. The objective of this thesis is to discuss the transient temperature behavior in the wellbore and surrounding formation and its impact on hydraulic fracturing.

In this paper, an efficient and accurate model for both the wellbore and the formation is developed using finite-difference method. The model is based upon the first principle of hydrodynamics and thermodynamics, and accounts for transient mass flow as well as thermal transfer to compute the temperature profile at any specific time and location during production. After model validation using Ramey's semi-analytical solution and Wu's transient heat transfer model, the model was used in a real deepwater production field to understand the impact of well production history on temperature. The simulation results indicate that not only the well shut in duration, production time, but also the flow rate history affect temperature transverse the wellbore.

Then the model is coupled with a fracture propagation model to study the temperature impact on hydraulic fracturing. Factors being considered include the rheology change on fracking fluid and the stress state change in the wellbore and formation. The temperature impact is shown by comparing the growth of fracture half-length and

fracture width with a normal fracture model. Both the single vertical fracture case and multistage hydraulic fracturing case are discussed.

Chapter 1: Introduction

1.1 Problem Statement

In a wellbore, the transient temperature behavior develops as the fluid (produced or injected) moves along the wellbore, exchanging heat with the surrounding formation, which results in changes of fluid in the wellbore and rock properties. This transient heat transfer between the wellbore and surrounding formation is generally defined by two processes: convection dominated heat transfer within the wellbore and conduction dominated heat transfer between pipe and surrounding and within formation.

Understanding this transient temperature behavior is critical for petroleum engineers in several aspects. For example, for hydrocarbon production in deepwater wells, the temperature difference between the seafloor and well bottomhole can be of several hundred Fahrenheit degrees. This temperature change may cause flow assurance problems such as wax deposition and hydrates formation.

Numerous studies have been done on the transient temperature behavior in wellbore and surrounding formation. Ramey (RAMEY JR 1962) proposed a 1-D cylindrical semi steady-state wellbore heat transfer model in which wellbore heat transfer is in steady state and heat transfer to formation is in transient state. Ramey's model assumes constant fluid flowing rate and cannot be used to solve rate transient problems. Hasan et al. (Hasan, Kabir et al. 2002) developed a numerical simulation model for transient heat analysis. However, their model requires many parameters that cannot be directly measured, including the overall heat transfer coefficient and relaxation distance. Igzec's (Izgec 2008) model is based on Hasan's work, and have the same disadvantages on

model complexity. Therefore, these models have limited capacity, and are difficult for field applications.

There is no current model available for decision making based on transient temperature behavior. Thus, an efficient and robust transient temperature model is needed to fill this gap.

1.2 Research Objective

The main objective of this thesis is to study the heat transfer processes and temperature impacts on wellbore fluids and surrounding formation in transient-rate condition, and particularly, to get a better understanding of the temperature distribution of the wellbore fluids, wellbore completion system and the surrounding formation. Specific objectives of this research are listed below:

(1) Develop a numerical simulation model for the transient heat behavior in wellbore and surrounding formation. This model combines convection in pipe strings and conduction in surrounding regions, and accounts for complex wellbore completions as well as heterogeneous reservoir formation conditions.

(2) Analyze the temperature distribution in wellbore and surrounding formations under different well schedules including rate-transient production periods and shut-ins.

(3) Study the temperature impacts on hydraulic fracturing caused by fracking fluid injection and wellbore and formation cooling processes.

1.3 Organization of Thesis

This thesis is consisted of eight chapters. Chapter 1 introduces the problem and research objective. Chapter 2 gives the background and previous research status of this topic. Chapter 3 describes the physical and mathematical model used in this thesis in the form of partial differential equations, and the detailed discretization is shown in this chapter.

The model validation for different scenarios and case study are in Chapter 4. Chapter 5 uses this model to analyze the temperature impact on hydraulic fracturing. Chapter 6 concludes this thesis and talks about future research steps.

Chapter 2: Literature Review

Transient temperature behavior develops as the fluid moves along the wellbore. Heat exchange mechanisms in the wellbore and surrounding formation include convection dominated heat transfer within the wellbore and conduction dominated heat transfer between pipe and surrounding and within formation.

Farris (Farris 1941) conducted studies of static and circulating temperature in five oil wells in the Gulf coast. He developed charts to correlate the bottom-hole wellbore temperature with depth. Farris's work has prompted researches into more accurate mathematical models for determining wellbore temperature.

Lesem et al. (Lesem, Greytok et al. 1957) derived one of the earliest heat transmission equations to describe the temperature behavior of gas and hot-water injection wells. However, Lesem's method ignored the conductive heat transfer in vertical direction, and neglected wellbore thermal resistance. He also assumed homogeneous and isotropic formation condition and constant thermal properties of fluids and formation.

Edwardson et al. (Edwardson, Girner et al. 1962) developed a heat transfer model for computing temperature changes in the formation caused by drilling fluid circulation. Their work was based on the mathematical solution of the heat conduction differential equations in a radial coordinates system. The solution of Edwardson's model was presented in graphical form to determine the spatial temperature distribution.

Ramey (RAMEY JR 1962) proposed a model to estimate the wellbore fluid temperature distribution based on a 1-D heat balance and uses an overall heat transfer coefficient for heat losses. Important assumptions for the model include constant flow rate within the

wellbore and steady state heat transfer through wellbore, which have limited the capacity of Ramey's model for field applications.

Willhite (Willhite 1967) suggested a method to determine the overall heat-transfer coefficient used in Ramey's model. His paper coupled multiple heat transfer mechanisms and presented the comparison of calculated and measured casing temperatures during steam injection.

Horne and Shinohara (Horne and Shinohara 1979) presented a single-phase heat transmission model based on Ramey's analysis and notation. Their model accounts for finite fluid flow rate and determines the heat-loss rate as a function of fluid properties and flow rate.

Shiu and Beggs (Shiu and Beggs 1980) developed an empirical correlation for producing oil wells to determine the relaxation distance used by Ramey. This work attempted to avoid the complex calculation of the overall heat-transfer coefficient in the wellbore and the transient heat-transfer behavior of the reservoir. Their work has become a valid simplification of Ramey's method.

Miller (Miller 1980) developed one of the earliest transient wellbore simulators, which accounts for changes in geothermal-fluid energy while flowing up the wellbore. In this model, mass and momentum equations are combined with the energy equation to yield an expression for pressure. After solving for pressure, density, energy, and velocity are calculated for the new timestep at a well gridblock.

Caslaw and Jaeger (Caslaw and Jaeger 1986) proposed comprehensive studies on heat conduction in solids. They presented numerous analytical equations to analyze the heat

conduction under different initial and boundary conditions. Their work has been widely accepted and used as the foundation to estimate temperature behavior in formation.

Sharma et al. (Sharma, Shoham et al. 1989) modified Ramey's equation for the case of producing wells with a downhole heater. Their work also relaxed Ramey's assumptions to a two-phase –flow condition.

Sagar et al. (Sagar, Doty et al. 1991) developed a simplified method suitable for hand calculations based on field data. His model predicts the temperature profiles in two-phase flowing wells assuming steady-state heat transfer within the wellbore.

Wu and Pruess (Wu and Pruess 1990) presented an analytical solution for wellbore heat transfer in layered formation in both real and Laplace space with different thermal properties. Their studies showed that the Ramey method was valid at late times but could get large errors at early times.

Santoyo-Gutierrez (Santoyo-Gutierrez 1997) proposed a study on transient heat transfer in geothermal well drilling process. He made comprehensive studies on convective heat transfer, and developed a simulator to estimate the temperature profile in wellbore and formation. However, his work is still limited to a steady-state mass rate assumption.

Hasan et al. (Hasan, Kabir et al. 2002) presented wellbore/reservoir simulators for gas, oil and two-phase flows. Their formulation consists of solution of coupled mass, momentum, and energy equations, all written in finite-difference form, and requires separate matrix operations. In all cases, the wellbore model is coupled with an analytic reservoir model.

Hagoort (Hagoort 2004) performed an analysis of the basic wellbore heat transmission equations and developed a rigorous solution. He compared the solution with Ramey

solution for various ranges of dimensionless numbers, and presented a simple graphical correlation to estimate the length of early transient period.

Izgec (Izgec 2008) later changed the form of Hasan and Kabir model. However, his work was still using complex overall heat-transfer coefficient and relaxation parameters, making the process time-consuming for real field data.

Chapter 3: Model for Wellbore and Surrounding Formation Heat Transfer

3.1 Schematics of Wellbore and Formation Model

A well is assumed to be placed vertically in an infinite cylindrical reservoir, and six different zones are identified from the center of wellbore to formation as shown in **Figure 1.** The description for every zone is as follows:

(1) The pipeflow zone, where the fluid is flowing inside tubing.

(2) The tubing zone.

(3) The annulus zone. The spacing between the production casing and tubing.

(4) The casing material zone.

(5) The cement zone, between casing and formation. As the cement usually has different thermal properties with the formation and pipe strings, it is necessary to define this zone separately.

(6) The formation zone. It is consisted of porous rock and fluids.

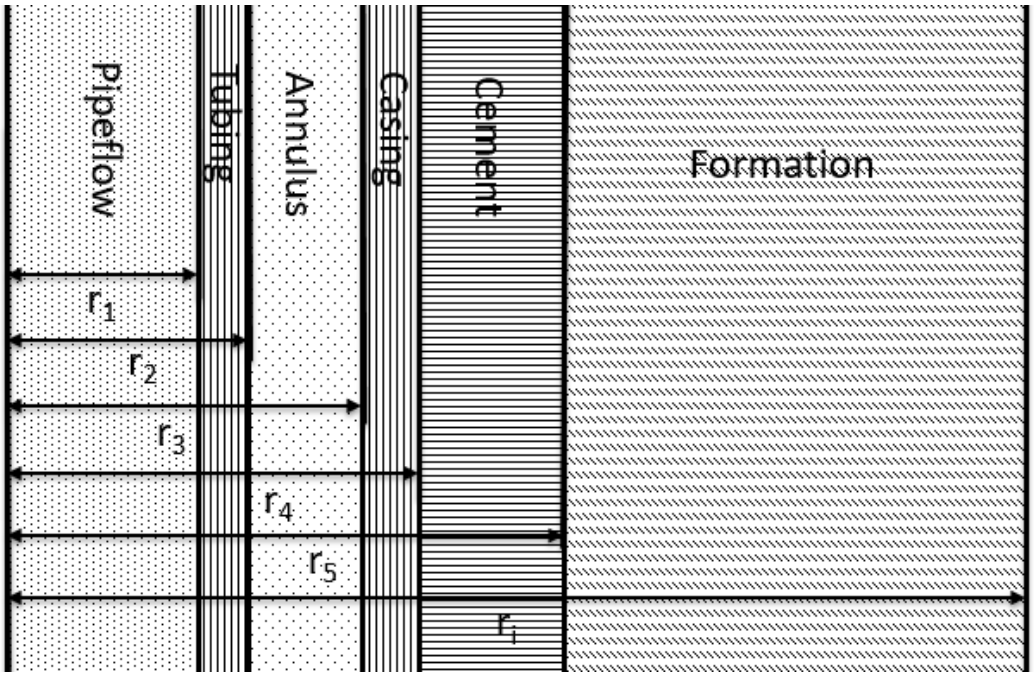

Figure 1 Structure of heat transfer model for wellbore and surrounding formation

The zones listed above are under different heat transfer processes. The pipeflow zone, with liquid flowing along the tubing, transfers heat with contacting tubing through convection. Convection also appears between the annulus zone and the contacting tubing and casing. On the other hand, the heat transfer inside tubing, casing, cement and formation are dominated by conduction.

As the formation is made up of porous media and liquid, more specifications must be made to describe the heat transfer process in this zone. **Appendix A** provides a detailed discussion about the temperature dependency and correlations used to estimate these properties**.** The heat conduction in solid and liquid phase are discussed in parallel, thus effective heat transfer properties are applied to calculate the temperature profile.

3.2 Mathematical Modeling of Transient Heat Transfer

3.2.1 Model Description

The following assumptions are made to set up the mathematical model:

(1) The well is flowing at a transient rate, and the fluid rate q can be described as a function of time t.

$$Q = Q(t) \tag{3.1}$$

(2) The Joule-Thompson effect is negligible during the analysis. This assumption has been verified by Prats (Prats 1982).

(3) Viscous dissipation is negligible. This assumption has been verified by Bird et al. (Bird, Stewart et al. 2007).

(4) Thermal expansion effect in the wellbore is negligible.

(5) No heat source or sink inside the wellbore or in the formation.

(6) The initial temperature in pipeflow, tubing, annulus, casing and cement regions are set to geothermal temperature.

$$T(r, z, \theta)_{t=0} = \psi(z) \tag{3.2}$$

(7) As the temperature distribution around a wellbore is axis-symmetric,

$$\frac{\partial T(t, r, z, \theta)}{\partial \theta} = 0 \tag{3.3}$$

A radial coordinate system is chosen to describe the physical model of the well and its surrounding formation. As the temperature profile along θ direction is not considered, the mathematical model is set up in a 2-D radial coordinate system.

3.2.2 Mathematical Modeling the Heat Transfer in the System

Applying energy balance on an open, unsteady-state flow system, we have:

$$\frac{\partial}{\partial t}\rho\left(U+\frac{1}{2}v^2\right)=-\left(\nabla\cdot\rho v\left(U+\frac{1}{2}v^2\right)\right)-\nabla\cdot q-\nabla\cdot(\tau\cdot v)-(\nabla\cdot pv)+\rho(v\cdot g) \quad (3.4)$$

The term on the left side of equation represents the rate of energy change per volume of the internal and kinetic energy, and U is the internal energy per unit mass, while the five terms on the right side represents: (1) the rate of increase of energy per volume due to convection, (2) the rate of energy increase due to molecular transport, (3) the rate of work done on the fluid by viscous forces, (4) the rate of work done on the fluid by pressure forces, and (5) the rate of work done on the fluid by gravitational forces, respectively.

For the internal energy of a constant control volume at a constant pressure,

$$dU = C_p dT \quad (3.5)$$

Combining (3.5) with (3.4), and applying the general assumption above to the governing energy balance equation, the differential equation is reduced to:

$$\frac{\partial}{\partial t}\left(\rho C_p T\right)=-\left(\nabla\cdot\rho v C_p T\right)-\nabla\cdot q \quad (3.6)$$

Converting this equation into the radial coordinate system defined above gives:

$$\frac{\partial}{\partial t}\left(\rho C_p T\right)=-\left[v_r\frac{\partial}{\partial r}\left(\rho C_p T\right)+v_z\frac{\partial}{\partial z}\left(\rho C_p T\right)\right]-\left[\frac{1}{r}\frac{\partial}{\partial r}\left(rq_r\right)+\frac{\partial q_z}{\partial z}\right] \quad (3.7)$$

For heat flux in the vertical and radial direction, Fourier's law gives:

$$q_z=-k_z\frac{\partial T}{\partial z} \quad (3.8)$$

$$q_r=-k_r\frac{\partial T}{\partial r} \quad (3.9)$$

Combining (3.8) and (3.9) with equation (3.7) gives the governing equation of heat flow in the form of (3.10):

$$\rho C_p\left(\frac{\partial T}{\partial t}+v_r\frac{\partial T}{\partial r}+v_z\frac{\partial T}{\partial z}\right)=\frac{k_r}{r}\frac{\partial T}{\partial r}+k_r\frac{\partial^2 T}{\partial r^2}+k_z\frac{\partial^2 T}{\partial z^2} \tag{3.10}$$

The continuity equation for liquid flow in this 2-D radial system is:

$$\frac{1}{r}\frac{\partial\left(rv_r\right)}{\partial r}+\frac{\partial v_z}{\partial z}=0 \tag{3.11}$$

The initial temperature profile is geothermal temperature, which is shown in (3.12).

$$T\left(r,z,t=0\right)=\psi\left(z\right) \tag{3.12}$$

The heat convection between fluid and the surface of pipe strings is modeled using Newton's law:

$$q=-h\left(T_m-T_f\right) \tag{3.13}$$

where h is the convective heat transfer coefficient. Derivation of this coefficient is discussed in **Appendix B**.

As there is no mass flux in the radial direction along the wellbore,

$$\left(\frac{\partial v_r}{\partial r}\right)_{z\neq z_{\max}}=0 \tag{3.14}$$

The vertical flowing velocity of fluid is a function of the well flowing history.

$$v_z\left(t\right)=\frac{Q\left(t\right)}{A_{pipe}} \tag{3.15}$$

The model has capability to handle injection problems as well as production problems. For production wells, the initial fluid temperature is set up at bottomhole location where $z=z_{\max}$,

$$T_f\left(r,t=0\right)_{z=z_{\max}}=T\left(r,t=0\right)_{z=z_{\max}} \tag{3.16}$$

For injection wells, the same governing equation still applies, but the fluid rate is changed to negative compared with the production case. The fluid temperature is set up to the injection temperature, which is measured at top surface.

$$T_f\left(r,t\right)_{z=0} = T_{inj}(t) \tag{3.17}$$

3.3 Numerical Discretization

A finite difference method is used to discretize the partial differentials implicitly. The diagram of the coordinate system and different regions is shown in **Figure 2**.

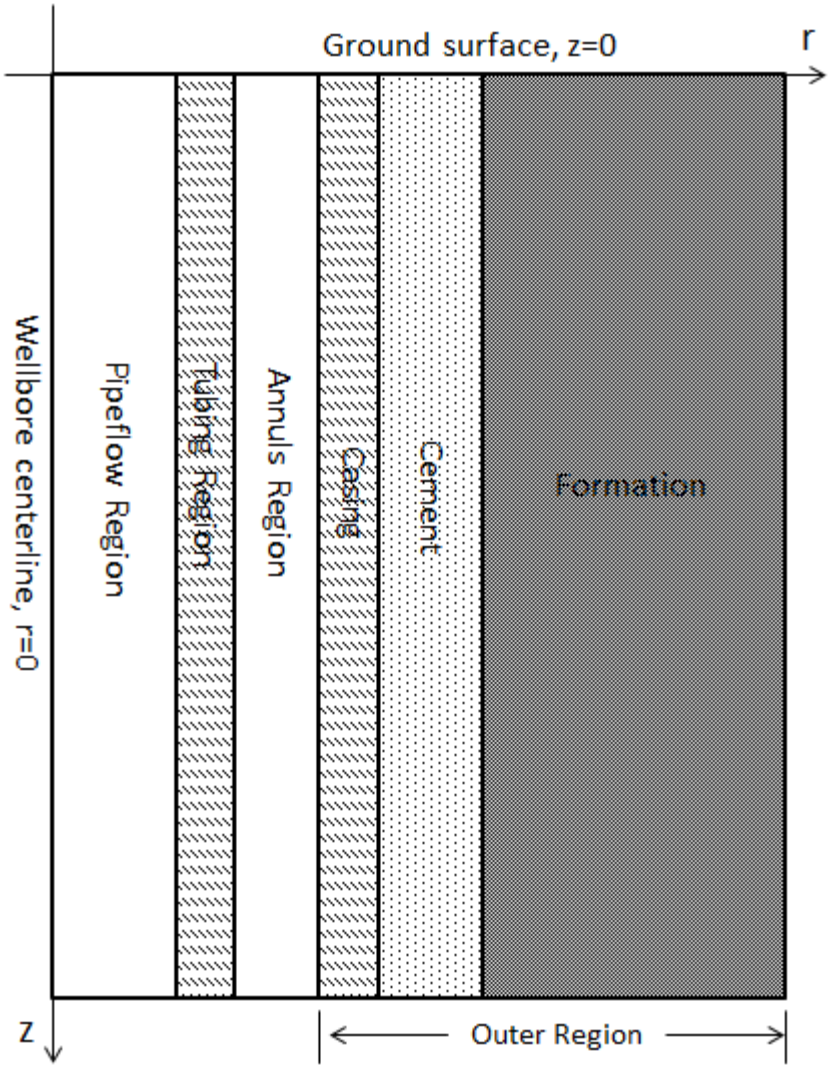

Figure 2 Coordinate system and region definition for model numerical discretization

For space discretization in *r* and *z* directions, the first order spatial discretization is:

$$\frac{\partial T}{\partial r} = \frac{T_{i+1,j}^{t+\Delta t} - T_{i-1,j}^{t+\Delta t}}{2\Delta r} \tag{3.18}$$

$$\frac{\partial T}{\partial z} = \frac{T_{i,j+1}^{t+\Delta t} - T_{i,j-1}^{t+\Delta t}}{2\Delta z} \tag{3.19}$$

The second order spatial discretization is:

$$\frac{\partial^2 T}{\partial r^2} = \frac{T_{i+1,j}^{t+\Delta t} - 2T_{i,j}^{t+\Delta t} + T_{i-1,j}^{t+\Delta t}}{\Delta r^2} \tag{3.20}$$

$$\frac{\partial^2 T}{\partial z^2} = \frac{T_{i,j+1}^{t+\Delta t} - 2T_{i,j}^{t+\Delta t} + T_{i,j-1}^{t+\Delta t}}{\Delta z^2} \tag{3.21}$$

Where *i* is the grid block on radial direction and *j* is the grid block on vertical direction.

For time discretization,

$$\frac{\partial T}{\partial t} = \frac{T_{i,j}^{t+\Delta t} - T_{i,j}^{t}}{\Delta t} \tag{3.22}$$

By discretizing the equations with finite difference method, the equations for every region can be conducted in a vector form of:

$$A_{i,j} T_{i,j-1}^{t+\Delta t} + B_{i,j} T_{i,j}^{t+\Delta t} + C_{i,j} T_{i,j+1}^{t+\Delta t} = D_{i,j} \tag{3.23}$$

which can be solved using tridiagonal algorithm.

Detailed discretization for different regions is shown in the sections below.

3.3.1 Pipeflow Region

For fluid flowing in the pipe (subscript 1), as no radial flow presents in the pipe, the governing equation (3.10) and continuity equation (3.11) are simplified to the form of:

$$\rho_1 C_{p1} \left(\frac{\partial T_1}{\partial t} + v_z \frac{\partial T_1}{\partial z} \right) = \frac{k_r}{r} \frac{\partial T_1}{\partial r} + k_r \frac{\partial^2 T_1}{\partial r^2} + k_z \frac{\partial^2 T_1}{\partial z^2} \tag{3.24}$$

$$\frac{\partial v_z}{\partial z} = 0 \tag{3.25}$$

The boundary condition is then changed to:

$$-k_{r1} \left(\frac{\partial T_1}{\partial r} \right)_{r=r_1} = h_1 \left(T_2 - T_1 \right) \tag{3.26}$$

To discretize this region, another boundary condition must be set up as:

$$\left(\frac{\partial T}{\partial r}\right)_{r=0} = 0 \tag{3.27}$$

And the radial temperature difference for fluid is also neglected.

$$\left(\frac{\partial T}{\partial r}\right)_{r\le r1} = 0 \tag{3.28}$$

The *A*,*B*,*C* and *D* are then discretized as shown below:

$$A_{1,j} = -v_{1,j}\left(\frac{\Delta t}{2\Delta z_j}\right) - \frac{k_{z1,j}}{\rho_{1,j}C_{p_{1,j}}}\left(\frac{\Delta t}{\Delta z_j^2}\right) \tag{3.29}$$

$$B_{1,j} = 1 + \left(\frac{2h_{1,j}}{r_1} + \frac{2k_{z1,j}}{\Delta z_j^2} + \frac{3k_{r1,j}}{r_1^2}\right)\left(\frac{\Delta t}{\rho_{1,j}C_{p_{1,j}}}\right) \tag{3.30}$$

$$C_{1,j} = v_{1,j}\left(\frac{\Delta t}{2\Delta z_j}\right) - \frac{k_{z1,j}}{\rho_{1,j}C_{p_{1,j}}}\left(\frac{\Delta t}{\Delta z_j^2}\right) \tag{3.31}$$

$$D_{1,j} = T_{1,j}^t + \left(\frac{2h_{1,j}}{r_i} + \frac{2k_{z1,j}}{\Delta z_j^2} + \frac{3k_{r1,j}}{r_1^2}\right)\left(\frac{\Delta t}{\rho_{1,j}C_{p_{1,j}}}\right)T_{2,j}^t \tag{3.32}$$

3.3.2 Tubing Region

For the steel pipe string (subscript 2), there is no flow presenting. Equation (3.10) is simplified to the form of:

$$\rho_2 C_{p2}\left(\frac{\partial T_2}{\partial t}\right) = \frac{k_r}{r}\frac{\partial T_2}{\partial r} + k_r\frac{\partial^2 T_2}{\partial r^2} + k_z\frac{\partial^2 T_2}{\partial z^2} \tag{3.33}$$

Besides (3.26), another boundary condition must be set up to model the heat convection between the tubing region and annulus fluid.

$$-k_{r3}\left(\frac{\partial T_3}{\partial r}\right)_{r=r_2} = h_2\left(T_2 - T_3\right) \tag{3.34}$$

The *A*,*B*,*C* and *D* are then discretized as shown below:

$$A_{2,j} = -\frac{k_{z2,j}}{\rho_{2,j} C_{p_{2,j}}} \left(\frac{\Delta t}{\Delta z_j^2} \right) \tag{3.35}$$

$$B_{2,j} = 1 + \left[\frac{2\left(h_{1,j} r_1 + h_{2,j} r_2\right)}{\left(r_2^2 - r_1^2\right)} + \frac{2k_{z2,j}}{\Delta z_j^2} + \frac{2k_{r2,j}}{r_1^2 + \frac{1}{2}\left(\frac{r_3 - r_2}{2}\right)^2} \right] \left(\frac{\Delta t}{\rho_{2,j} C_{p_{2,j}}} \right) \tag{3.36}$$

$$C_{2,j} = -\frac{k_{z2,j}}{\rho_{2,j} C_{p_{2,j}}} \left(\frac{\Delta t}{\Delta z_j^2} \right) \tag{3.37}$$

$$D_{2,j} = T_{2,j}^t + \left[\frac{2h_{1,j} r_1 T_{1,j}^t + 2h_{2,j} r_{out} T_{3,j}^t}{r_2^2 - r_1^2} + \frac{2k_{2,j}\left(T_{1,j}^t + T_{3,j}^t\right)}{r_1^2 + \frac{1}{2}\left(\frac{r_3 - r_2}{2}\right)^2} - \frac{k_{2,j}\left(T_{3,j}^t - T_{1,j}^t\right)}{\left(\frac{r_3 + r_2}{2}\right)\left(r_1^2 + \frac{r_3 - r_2}{2}\right)} \right] \left(\frac{\Delta t}{\rho_{2,j} C_{p_{2,j}}} \right) \tag{3.38}$$

3.3.3 Annulus Region

For the fluid flowing in the annulus (subscript 3), the governing equation (3.10) is simplified to the form of:

$$\rho_3 C_{p3} \left(\frac{\partial T_3}{\partial t} + v_z \frac{\partial T_3}{\partial z} \right) = \frac{k_r}{r} \frac{\partial T_3}{\partial r} + k_r \frac{\partial^2 T_3}{\partial r^2} + k_z \frac{\partial^2 T_3}{\partial z^2} \tag{3.39}$$

$$\frac{1}{r} \frac{\partial \left(r v_r\right)}{\partial r} + \frac{\partial v_z}{\partial z} = 0 \tag{3.40}$$

The heat convection between the annulus fluid and contacting completion materials is modeled as:

$$-k_{r3} \left(\frac{\partial T_3}{\partial r} \right)_{r=r_3} = h_3 \left(T_4 - T_3 \right) \tag{3.41}$$

The *A*,*B*,*C* and *D* are expressed in below:

$$A_{3,j} = -v_{3,j} \left(\frac{\Delta t}{2\Delta z_j} \right) - \frac{k_{z3,j}}{\rho_{3,j} C_{p_{3,j}}} \left(\frac{\Delta t}{\Delta z_j^2} \right) \tag{3.42}$$

$$B_{3,j} = 1 + \left[\frac{2\left(h_{2,j} r_2 + h_{3,j} r_3\right)}{\left(r_3^2 - r_2^2\right)} + \frac{2k_{z3,j}}{\Delta z_j^2} + \frac{2k_{r3,j}}{\left(\frac{r_3 - r_2}{2}\right)^2} \right] \left(\frac{\Delta t}{\rho_{3,j} C_{p_{3,j}}} \right) \tag{3.43}$$

$$C_{3,j} = -v_{3,j} \left(\frac{\Delta t}{2\Delta z_j} \right) + \frac{k_{z3,j}}{\rho_{3,j} C_{p_{3,j}}} \left(\frac{\Delta t}{\Delta z_j^2} \right) \tag{3.44}$$

$$D_{3,j} = T_{3,j}^t + \left[\frac{2h_{2,j} r_2 T_{2,j}^t + 2h_{3,j} r_3 T_{4,j}^t}{r_3^2 - r_2^2} + \frac{k_{3,j}\left(T_{2,j}^t + T_{4,j}^t\right)}{\left(\frac{r_3 - r_2}{2}\right)^2} + \frac{k_{3,j}\left(T_{4,j}^t - T_{2,j}^t\right)}{\left(r_3 - r_2\right)\left(r_2 + \frac{r_3 - r_2}{2}\right)} \right] \left(\frac{\Delta t}{\rho_{3,j} C_{p_{3,j}}} \right) \tag{3.45}$$

3.3.4 Outer Region

While contacting with the annulus fluid, temperature behavior in the casing, cement and formation are all conduction only. To solve the problem, it is firstly required to write the energy equation at the contacting surface (subscript 4) between annulus and casing:

$$-k_{r3} \left(\frac{\partial T_3}{\partial r} \right)_{r=r_3} = h_3 \left(T_4 - T_3 \right) = -k_{r5} \left(\frac{\partial T_5}{\partial r} \right)_{r=r_3} \tag{3.46}$$

This can be written in a discretized form of:

$$T_{4,j}^{t+\Delta t} = \left[\frac{h_{3,j} + \frac{k_{3,j}}{r_3 - r_2}}{h_{3,j} + \frac{k_{3,j}}{r_4 - r_3} + \frac{k_{3,j}}{r_3 - r_2}} \right] T_{3,j}^{t+\Delta t} + \left[\frac{\frac{k_{5,j}}{r_4 - r_3}}{h_{3,j} + \frac{k_{5,j}}{r_4 - r_3} + \frac{k_{3,j}}{r_3 - r_2}} \right] T_{5,j}^{t+\Delta t} \tag{3.47}$$

Governing equations in the outer region are

$$\rho_5 C_{p5} \left(\frac{\partial T_5}{\partial t} + v_r \frac{\partial T_5}{\partial r} \right) = \frac{k_r}{r} \frac{\partial T_5}{\partial r} + k_r \frac{\partial^2 T_5}{\partial r^2} + k_z \frac{\partial^2 T_5}{\partial z^2} \tag{3.48}$$

$$\frac{\partial \left(r v_r \right)}{\partial r} = 0 \tag{3.49}$$

As the formation is made up of porous rock, effective thermal conductivity is calculated based on formation porosity and thermal properties of rock and fluid. When calculating the thermal conductivity of casing and cement, simply change the porosity to zero.

$$k_{5,j} = k_{rock}^{\phi} k_{fluid}^{1-\phi} \tag{3.50}$$

The *A,B,C* and *D* are expressed in below, note that the direction of heat conduction includes both radial and vertical:

$$A_{5,j} = -\frac{k_{5,j}}{\left(\rho_{5,j} C_{p_{5,j}}\right)}\left(\frac{\Delta t}{\Delta z_j^2}\right) \tag{3.51}$$

$$B_{5,j} = 1 + \frac{k_{5,j}}{\left(\rho_{5,j} C_{p_{5,j}}\right)}\left(\frac{\Delta t}{\Delta z_j^2}\right) \tag{3.52}$$

$$C_{5,j} = \frac{k_{5,j}}{\left(\rho_{5,j} C_{p_{5,j}}\right)}\left(\frac{\Delta t}{\Delta z_j^2}\right) \tag{3.53}$$

$$D_{5,j} = T_{5,j}^t + \left[\left(\frac{\Delta t}{\Delta r_5^2 + \Delta r_4^2}\right)\left(T_{6,j}^t - T_{5,j}^t\right)\right]\left(\frac{k_{5.j}}{\left(\rho_{5,j} C_{p_{5,j}}\right)}\right) \tag{3.54}$$

Chapter 4: Model Validation and Case Study

4.1 Ramey's Model

To make a valid comparison with Ramey's model, the following assumptions must be applied to the current model so that Ramey's model can be applied:

(1) The well is flowing in a constant rate.

(2) Formation properties are homogeneous and isotropic in all directions.

(3) The well has an infinite length for fluid flow.

(4) The fluid is single phase Newtonian fluid.

(5) The heat flux along mass flow direction is neglected.

In Ramey's model, the temperature distribution in a well with constant liquid rate is described as:

$$\frac{dT}{dz} = \frac{T - T_g}{A_R} \tag{4.1}$$

Where A_R is calculated as:

$$A_R = \frac{mC_p\left[f(t) rU_o + k \right]}{2\pi r U_o k} \tag{4.2}$$

Where $f(t)$ is the time-function, given graphically by **Figure 3**.

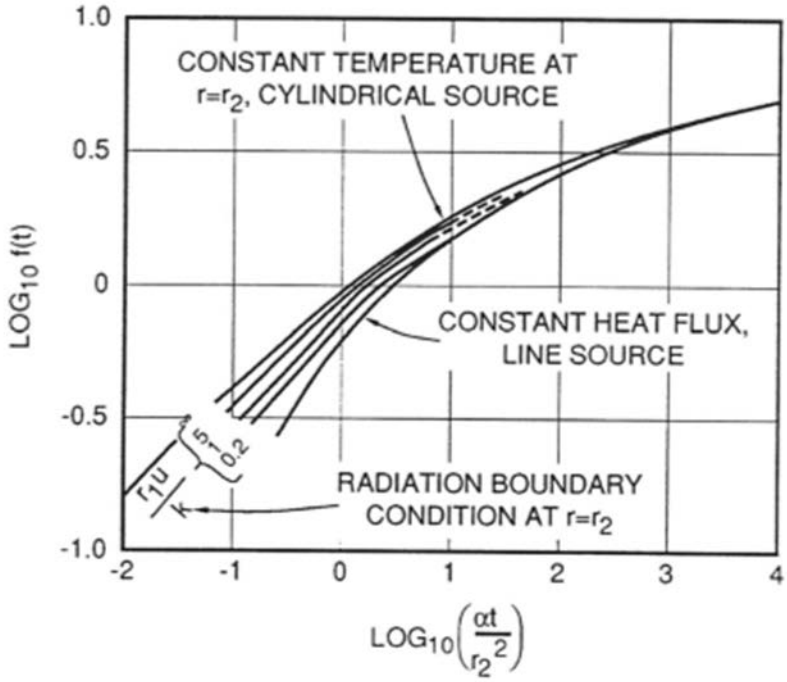

Figure 3 Time function for Ramey's model (Economides 1987)

For later times, when $\log_{10}\left(\frac{\alpha t}{r^2}\right) > 2.5$, Ramey's model has shown good accuracy, and the time function can then be approximated by a line-source solution that

$$f(t) = -\ln\left(\frac{r}{2\sqrt{\alpha t}}\right) - 0.290 \tag{4.3}$$

The overall heat transfer coefficient *U* can be calculated using McAdams (McAdams 1958) method. For a wellbore,

$$\frac{1}{U_o} = \frac{dA_1}{h_1 dA_1} + \frac{\Delta r_1 dA_1}{k_1 dA_2} + \frac{dA_1}{h_2 dA_3} + \frac{dA_1}{h_2 dA_4} + \frac{\Delta r_2 dA_1}{k_2 dA_5} + \cdots \tag{4.4}$$

To conduct the validation, input parameters for a case study are summarized in **Table 1** and the formation, fluid and tubing has the following thermal properties shown in **Table 2**. Note that the injection period is 75 days, and the late-time period has been reached.

Liquid Rate (m^3/d)	79.5
Well Depth (*m*)	1525
Casing OD (m)	0.178
Liquid Injection Temperature ($^\circ$ C)	14.7
Surface Temperature ($^\circ$ C)	21.2
Geothermal Gradient ($^\circ$ C/m)	0.015
Injection Period (*Days*)	75

Table 1 Validation well schedule for Ramey's model

	k (W/m° C)	C_p (J/Kg° C)	ρ (kg/m^3)	μ (Pa · s)
Formation	2.25	880.0	2640.0	Not Applied
Casing	43.33	418.7	8048.0	Not Applied
Fluid	0.59	4002.0	1000.0	0.0011

Table 2 Validation well thermal properties for Ramey's model

Figure 4 shows the comparison result between numerical simulation and Ramey's model. The match between Ramey and this heat transient simulation model is generally good, telling that the model is validated based on Ramey's assumptions and conditions.

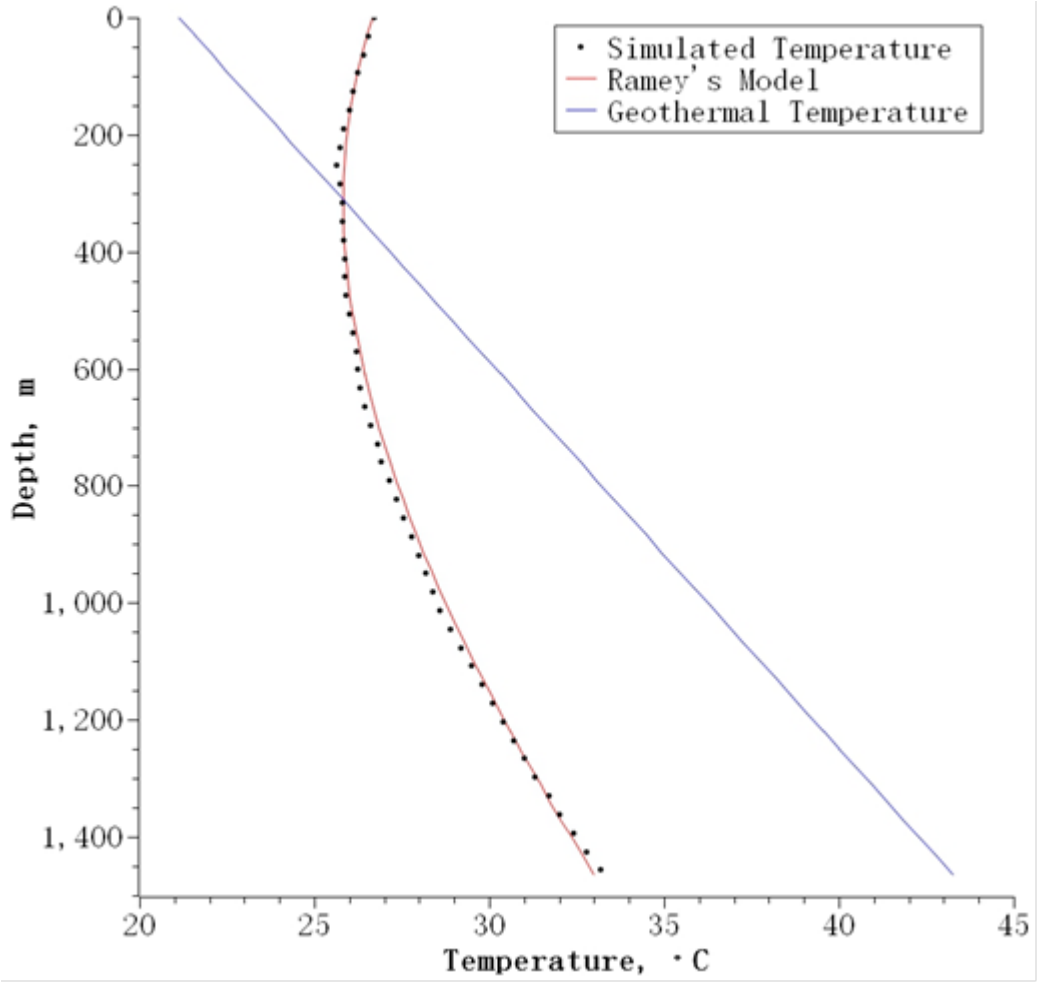

Figure 4 Model validation using Ramey's assumption

4.2 Analytical Transient Heat Model

Wu et al. (Wu, Xu et al. 2015) published an analytical model for transient heat behavior in wellbore. Their work performs a well shut-in process after producing and identifies the temperature distribution with respect to time and location.

To make validation using this transient heat model, following assumptions are to be made on the current model:

(1) Single liquid phase in tubing.

(2) Heat conduction in vertical direction is neglected.

(3) The thermal properties of formations are constant.

(4) The well is producing at steady-state.

From Wu et al. (Wu, Xu et al. 2015), the temperature at the wellbore is a function of flowing time and shut-in durations, shown in:

$$T_D\left(1,t_{Ds},t_{Dc}\right)=\frac{1}{2t_{Ds}}\int_0^{\infty}\exp\left[-\frac{\left(\tau-1\right)^2}{4t_{Ds}}\right]I_{0e}\left(\frac{\tau}{2t_{Ds}}\right)f_D\left(\tau,t_{Dc}\right)\tau d\tau \tag{4.5}$$

They solved the equation based on the line-source solution proposed by Kutasov (Kutasov 1989). The solutions are shown in below:

$$T_D\left(1,t_{Ds},t_{Dc}\right)=\begin{cases}\dfrac{\ln\left(1+1.3\dfrac{t_{Dc}}{t_{Ds}}\right)-\dfrac{0.25}{t_{Ds}}}{\ln\left(2.92t_{Dc}\right)}, t_{Ds}>0.5\\ \dfrac{a+b\ln\left(t_{Ds}\right)+c\ln\left(t_{Dc}\right)}{1+d\ln\left(t_{Ds}\right)+e\ln^2\left(t_{Ds}\right)+f\ln^3\left(t_{Ds}\right)+g\ln\left(t_{Dc}\right)}, t_{Ds}\le 0.5\end{cases} \tag{4.6}$$

Where factors from *a* to *g* are shown in **Table 3**.

a	b	c	d	e	f	g
0.5694	-0.1060	0.2763	0.2819	0.1155	0.0112	0.2747

Table 3 Factors used in Wu's model (Wu, Xu et al. 2015)

To conduct the validation, the input parameters for this study are summarized in **Table 4** and **Table 5**.

	k (W/m° C)	C_p (J/Kg° C)	ρ ($kg/$ m^3)	μ (Pa · s)
Formation	2.25	880.0	2640.0	Not Applied
Casing	43.33	418.7	8048.0	Not Applied
Fluid	1.15	2180.0	900.0	0.00096

Table 4 Validation data of thermal properties for Wu's model

Wellbore Radius (m)	0.198
Gauge Location (*m*)	5643
Tubing ID (m)	0.059
Sea Water Depth (m)	2080
Surface Temperature ($^{\circ}$ C)	21.2
Geothermal Gradient ($^{\circ}$ C/*m*)	0.018
Injection Period (*Days*)	11.67
Liquid Rate (m^3/d)	2225.8

Table 5 Validation data of well schedule and completion for Wu's model

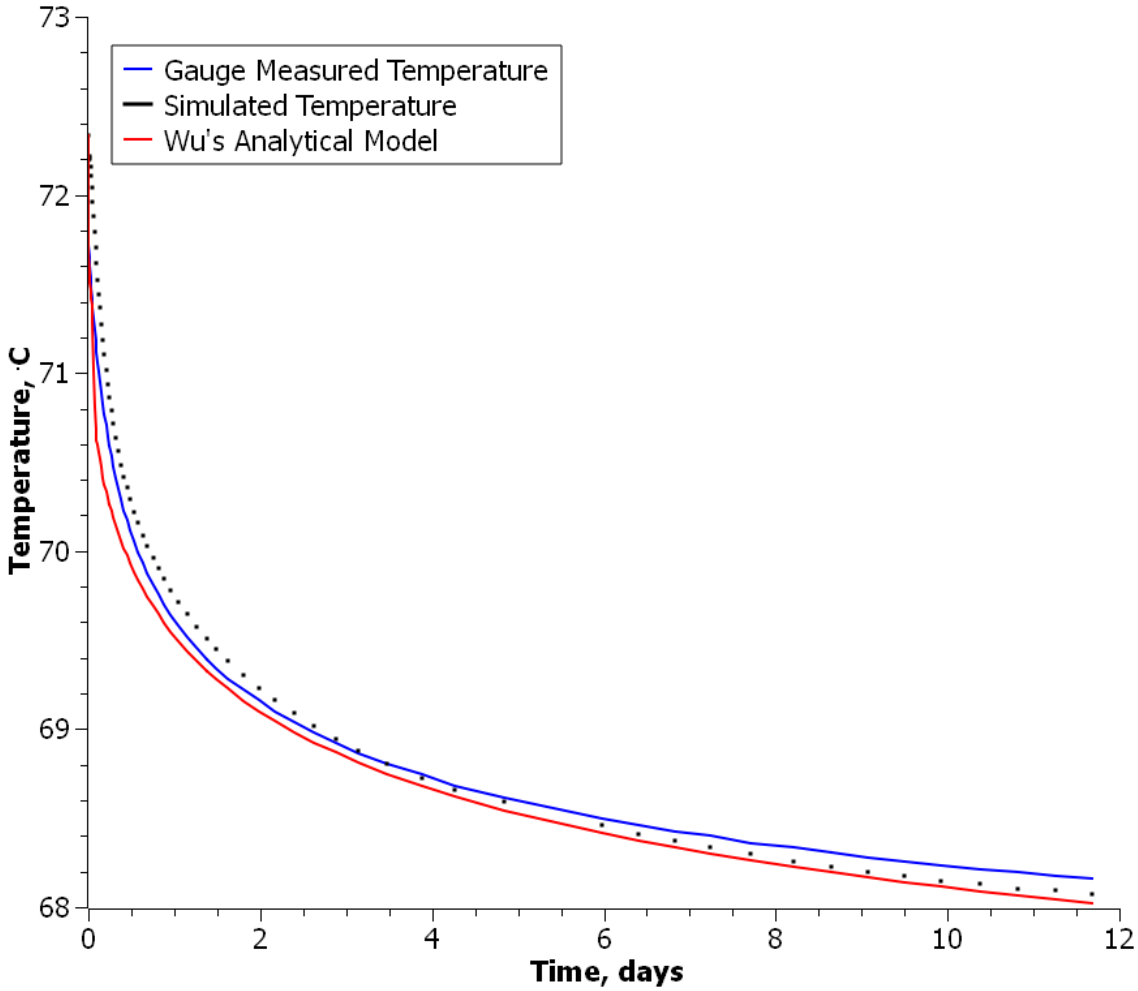

Figure 5 Validation with gauge data and Wu's model

Figure 5 shows the comparison result between numerical simulations, original gauge measured temperature data and Wu's model. The match between Wu's model and the current simulation model is generally good, telling that the model is validated.

When compared with gauge data, Wu's model performs slightly better than this current simulation model in early times, but worse in later times. The differences may come from the heat convection, which has been neglected by Wu et al.(Wu, Xu et al. 2015), but considered in the current simulation model.

4.3 Case Study for a Deepwater Well

An intelligent well with downhole pressure and temperature in Gulf of Mexico is used for case study using the developed simulation model. The wellbore diagram is shown in **Figure 6**.

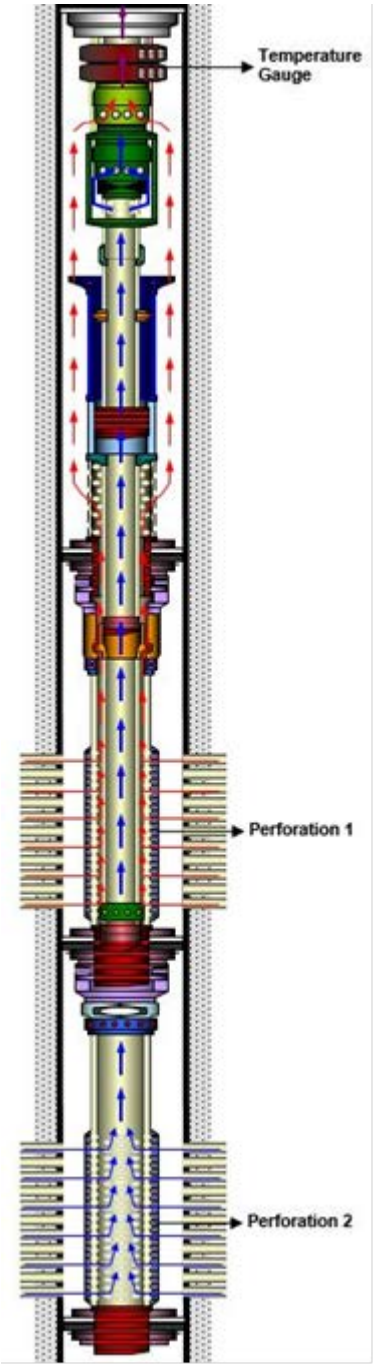

Figure 6 Wellbore diagram of case study well, a deepwater well in Gulf of Mexico

The well was completed and perforated at two different measured depths, 5245 and 5335 meters, respectively from Kelly Bushing. A temperature gauge was placed at the measured depth of 5005 m, from which the real temperature data was recorded.

The well has a production history shown in **Figure 7**. It has been producing at transient rates, and several shut-ins have been performed during the production history. **Table 6** and **Table 7** summaries the thermal properties for the well and the formation and input parameters used in this case study.

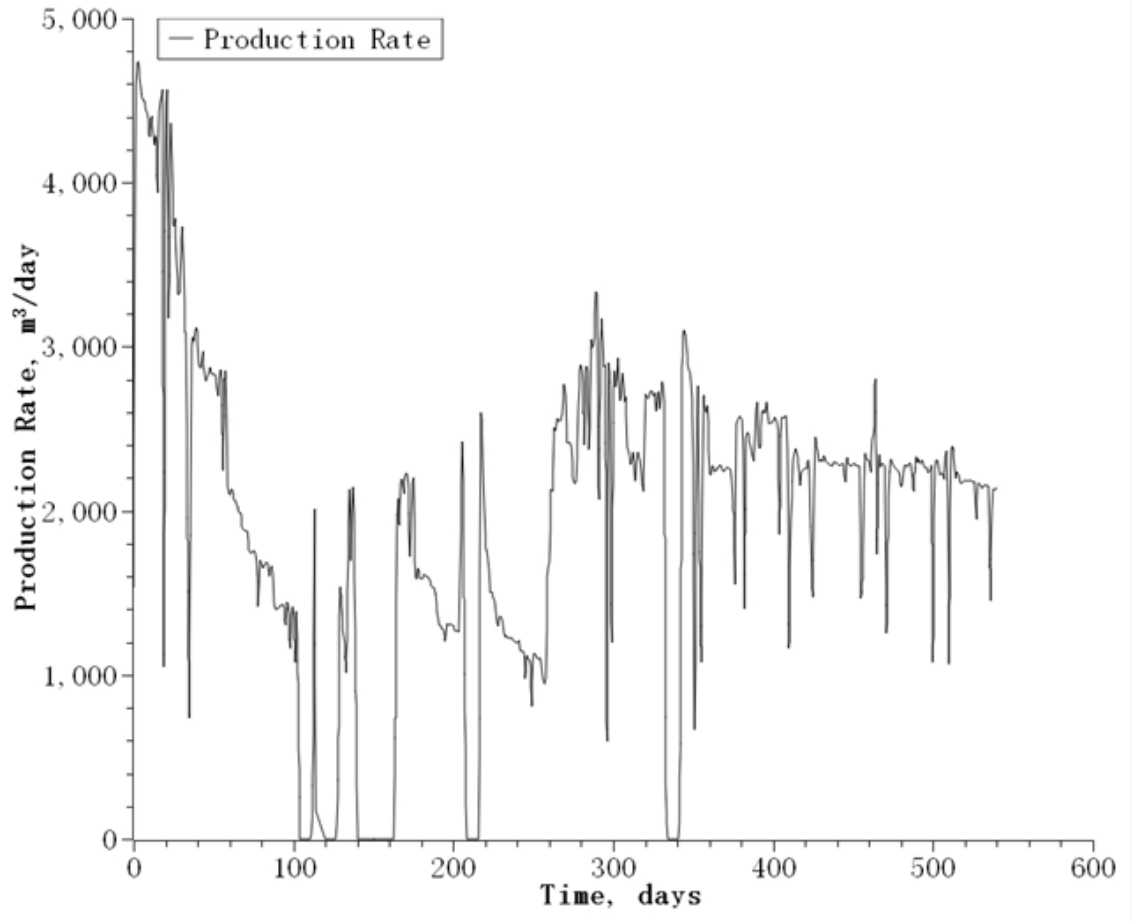

Figure 7 Production history of the case study well, a deepwater well in Gulf of Mexico

	k (W/m° C)	C_p (J/Kg° C)	ρ (kg/m^3)	μ (Pa · s)
Formation	2.25	880	2640	Not Applied
Tubing	43.33	418.7	8048.0	Not Applied
Fluid	1.15	1600.0	830.0	0.0096
Cement	0.70	2000.0	3140.0	Not Applied

Table 6 Thermal properties for the well of case study, in Gulf of Mexico

Gauge Depth (m)	5005
Perforation 1 Depth (m)	5245
Perforation 2 Depth (m)	5335
Tubing OD (m)	0.140
Surface temperature (℃)	23.20
Geothermal Gradient (℃/m)	0.009
Formation Porosity (ϕ)	0.2

Table 7 Well properties for the well of case study, in Gulf of Mexico

Studies are proposed to estimate the temperature profile at different depth both vertically along the wellbore and radially in the formation.

4.3.1 History Temperature Profiling

Simulation has been performed based on the data above, and the simulated temperature and recorded real temperature history are compared in **Figure 8**.

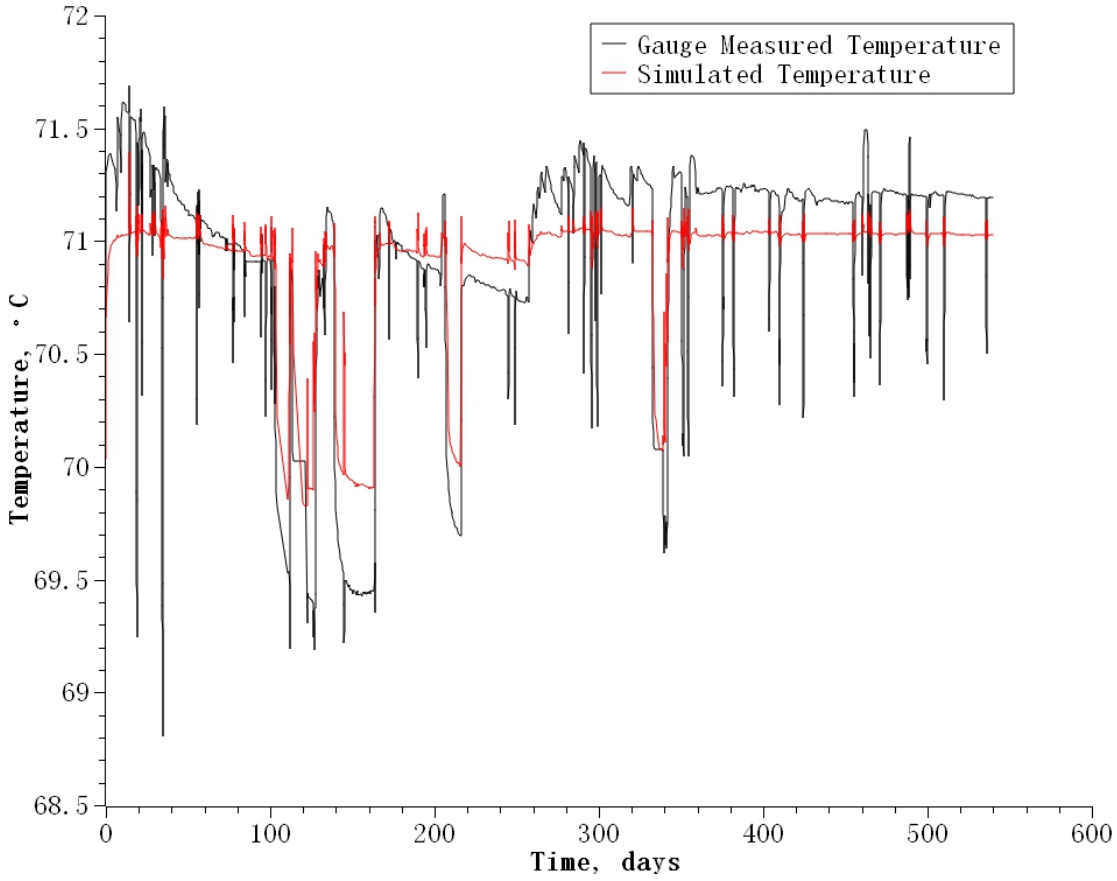

Figure 8 Temperature history profile at gauge location of case study, a deepwater well in Gulf of Mexico

The simulated results match the measured temperature with an average difference of less than 0.25ºC. The possible reasons attribute to the difference include:

(1) Reservoir dip angle. As the real fluid temperature flowing into the well is unknown, we used a constant flowing temperature for the whole history. However, the original reservoir has a dip angle of 70º, and the flowing temperature into the wellbore may be different.

(2) Joule-Thomson effect is neglected in the simulation. As pressure loss is not included in the simulator, the Joule-Thomason effect as the result of pressure changes is not considered.

(3) Temperature dependent property modelling. The methods used in modelling the thermal properties changes may not accurately model the real property changes because of temperature change.

(4) The gauge error: The gauge measurement has mechanical problems such as erroneous measurement and gauge measurement drift. All these factors lead to measurement errors.

(5) Non-linear geothermal temperature gradient. In the modelling process, a constant geothermal temperature gradient is assumed; however, the geothermal temperature gradient may not be a constant, especially in the deepwater environment in Gulf of Mexico.

In summary, the match quality is acceptable given there are so many possible reasons contributing to errors.

4.3.2 Radial Temperature Profiling

A study is proposed to estimate the temperature in the surrounding formation with respect to production time and distance to the wellbore center. The result is shown in **Figure 9**.

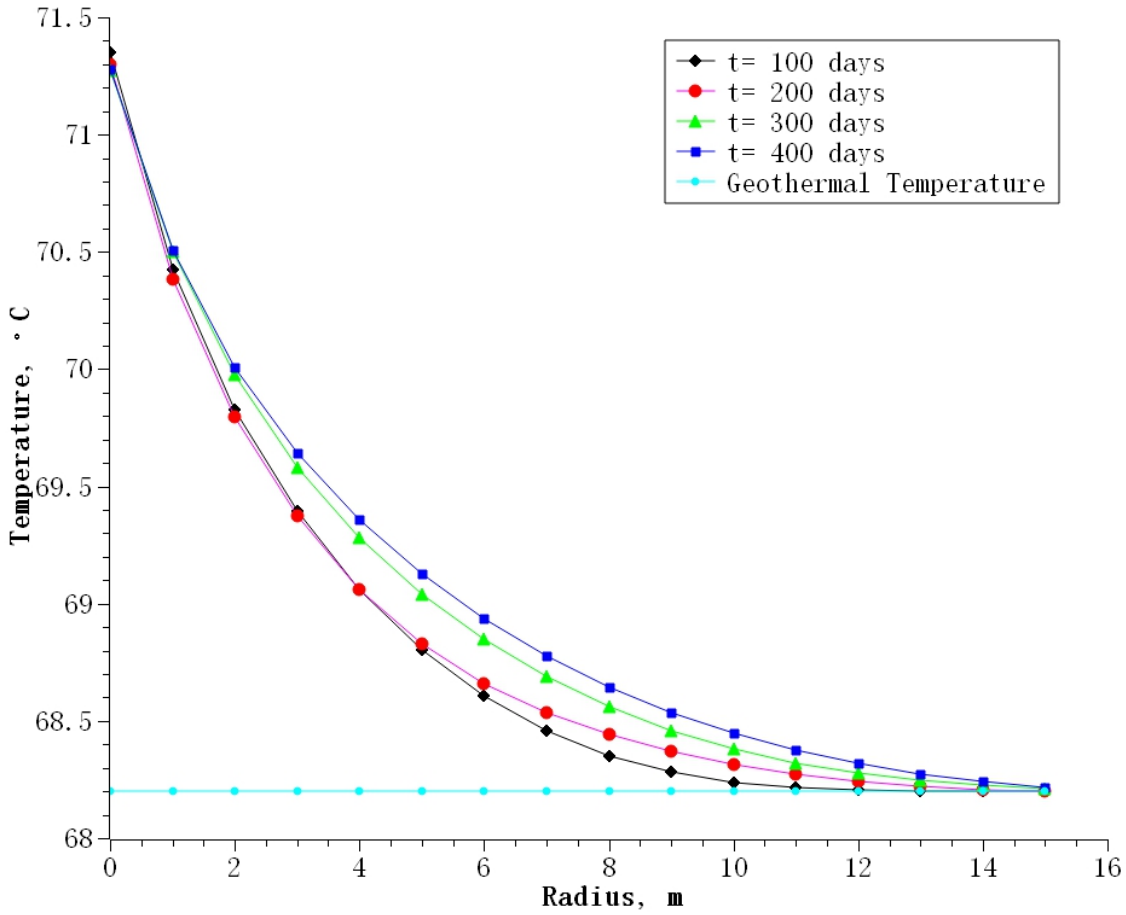

Figure 9 Temperature profile along radial direction of case study, a deepwater well in Gulf of Mexico

At the gauge depth (5005 m), as the well continues producing, the wellbore and near wellbore regions are heated through this process. Temperature at wellbore raises up continuously, until a constant temperature around 71.36 ºC is achieved after a period of producing, while the temperature in the surrounding formation slowly increases with time. Temperature in the formation outside the radius of 14.97 m remains unaffected at all times.

Chapter 5: Temperature Impacts on Hydraulic Fracturing

5.1 Heat Transfer during Hydraulic Fracturing

The heat transfer process during a hydraulic fracturing process happen when the pumping starts, as the cold fracturing fluid interacts with high-temperature formation by convection and conduction. Meyer (Meyer 1989) has studied the heat transfer during hydraulic fracturing. By solving the coupled continuity and energy-balance equations for an infinitesimal element of fluid in time and space, he modeled the dimensionless temperature in the fracture, shown in **Figure 10**.

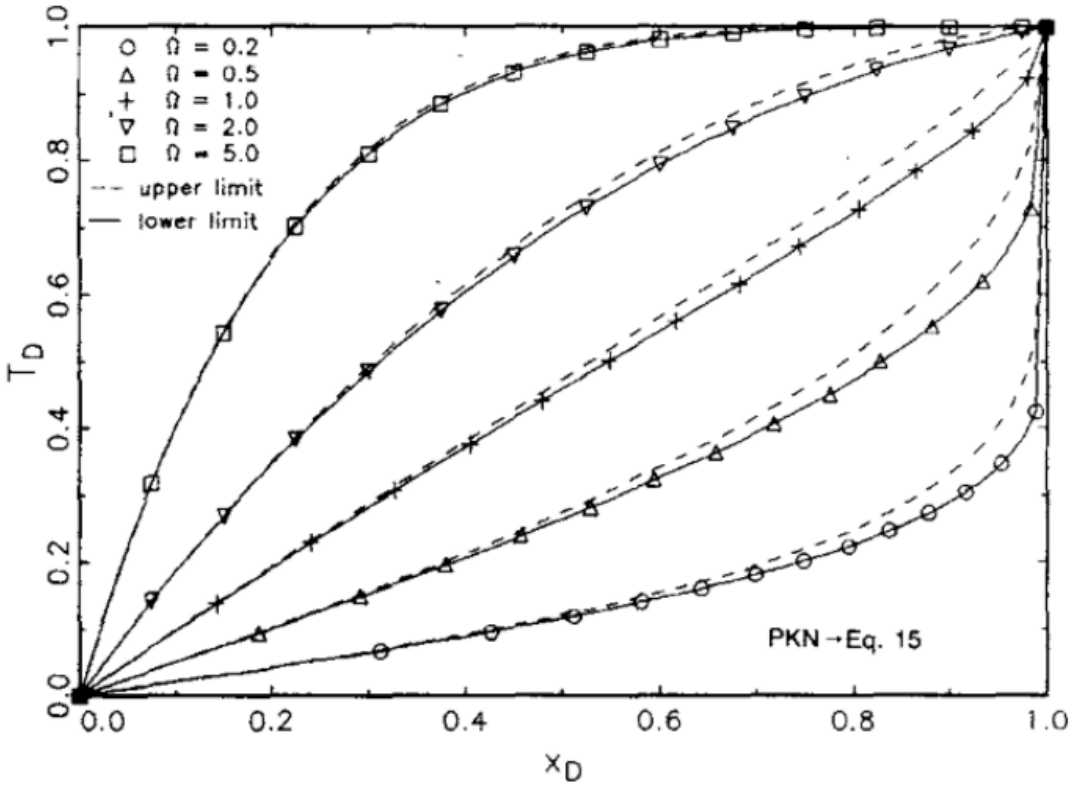

Figure 10 Dimensionless temperature profile in the fracture (Meyer 1989)

As the fracturing fluid invading formation rock, it receives energy influx from the high-temperature formation. Thus, the further fluid is transported in the fracture, the higher the temperatures it reaches.

Many other heat transfer models for hydraulic fracturing have been set up. Dysart (Dysart and Whitsitt 1967) published an analytical model for the fluid temperature in fractures. For a constant leak-off, Wheeler (Wheeler 1969) related temperature as a function of time and position to injection conditions and reservoir position to injection conditions and reservoir characteristics. Whitsitt (Whitsitt and Dysart 1970) studied the heat transfer during hydraulic fracturing with a linearly increasing leak-off factor.

In this chapter, the same temperature simulator is used to analyze the heat transient behavior during hydraulic fracturing, and the impacts of temperature on hydraulic fracturing are studied based on the propagation length and width of fractures.

5.2 Fracture Fluid Viscosity

Designing fracturing fluid properly is one of the key factors for a successful hydraulic fracturing process. During the process, good viscosity of fracturing fluid is required to provide proppant transport along the fracture. However, high viscosity may lead to the significant increase of net pressure, and causes height growth, leading to less penetration than expected. As the fracturing fluid properties are being affected by the temperature, the transient temperature behavior may cause variations in fluid properties and rheology, leading to unexpected results for hydraulic fracturing.

For brine-based fracturing fluids, the viscosity of fracturing fluid varies mainly with the pressure, temperature and salinity. Kestin (Kestin, Khalifa et al. 1981) proposed the

following model which is used to study the viscosity change for brine with respect to temperature behavior during hydraulic fracturing.

$$\mu(p,T,m)=\mu^{0}(T,m)\left[1+\beta(T,m)\cdot p\right] \tag{5.1}$$

Where the hypothetical zero-pressure viscosity μ^{0} is calculated by

$$\log_{10}\left[\mu^{0}(T,m)/\mu_{w}^{0}(T)\right]=A(m)+B(m)\log_{10}\left[\mu_{w}^{0}(T)/\mu_{w}^{0}(20^{\circ}C)\right] \tag{5.2}$$

$$\log_{10}\left[\mu_{w}^{0}(T)/\mu_{w}^{0}(20^{\circ}C)\right]=\sum_{i=1}^{4}\alpha_{i}\left[(20-T)/(96+T)\right] \tag{5.3}$$

$$A(m)=\sum_{i=1}^{3}a_{i}m^{2} \tag{5.4}$$

$$B(m)=\sum_{i=1}^{3}b_{i}m^{2} \tag{5.5}$$

and β is pressure coefficient.

$$\beta(T,m)=\left[\gamma_{0}+\gamma_{1}T-\sum_{i=0}^{4}\beta_{wi}T^{i}\right]\cdot\sum_{i=1}^{3}\beta_{i}\left(m/\left(\sum_{i=0}^{2}m_{i}T^{i}\right)\right)^{i}+\sum_{i=0}^{4}\beta_{wi}T^{i} \tag{5.6}$$

Where $a_{i},b_{i},\alpha_{i},\beta_{i},\beta_{wi},\gamma_{i}$ are constants listed in Kestin's publication, $\mu_{w}{}^{0}(20^{\circ}C)$ is equal to $1002Pa\cdot s$.

5.3 Thermal Stress

To estimate the total formation stress, it is necessary to include the thermal stresses by independent calculation and superposing on the normal stresses.

Gogoi (Gogoi 1986) performed a comprehensive study estimating the thermal stresses around a wellbore.

$$\sigma_{r,th}=\frac{\alpha_{l}E}{1-\nu}\left(T_{m}-T_{f,u}\right)\left[\frac{\ln r_{D}}{2\ln R_{D}}-\frac{1}{2}\left(1-\frac{1}{r_{D}{}^{2}}\right)\left(1+\frac{1}{2\ln R_{D}}\right)\right] \tag{5.7}$$

$$\sigma_{\theta,th} = \frac{-\alpha_l E}{1-\nu}\left(T_m - T_{f,u}\right)\left[1 - \frac{\ln r_D}{2\ln R_D} - \frac{1}{2}\left(1 - \frac{1}{r_D{}^2}\right)\left(1 + \frac{1}{2\ln R_D}\right)\right] \tag{5.8}$$

$$\sigma_{z,th} = \frac{-\alpha_l E}{1-\nu}\left(T_m - T_{f,u}\right)\left[1 - \frac{\ln r_D}{\ln R_D}\right] \tag{5.9}$$

Where $\sigma_{r,th}$, $\sigma_{\theta,th}$ and $\sigma_{z,th}$ are thermal stress components in cylindrical coordinates. T_m is the wellbore temperature and $T_{f,u}$ is the undisturbed formation temperature. r_D is the dimensionless radial distance measured in the unit of wellbore radius, and R_D is the dimensionless radius of thermal influence. α_l is the thermal linear expansion coefficient.

5.4 Hydraulic Fracture Propagation with Temperature Impact

To analyze the overall temperature impact on hydraulic fracturing, the following assumptions are addressed:

(1) The fracture geometry is PKN.

(2) Constant fluid leak-off coefficient.

(3) The hydraulic fracture fully penetrates the formation in vertical direction.

(4) The formation is under normal stress regime. Fracture propagates along minimum horizontal stress direction.

(5) Constant surface temperature and fluid pumping temperature during the process.

(6) Constant pumping rate at surface.

(7) The formation is homogeneous and isotropic.

A case study is performed to study the temperature impact on fracture propagation by coupling the previous mechanisms. A vertical well is placed in the reservoir, contacting with the top surface of a normal faulting shale formation, with a permeability of 100nD. Hydraulic fracturing is performed at bottomhole using brine, with a salinity of 35 ppt.

The procedure of case study is listed in below:

(1) Model the temperature behavior during pumping.

(2) Calculate fracking fluid viscosity change based on the temperature distribution at every pumping step.

(3) Calculate the pore pressure and normal stress state of formation.

(4) Calculate the thermal stress at every pumping step and superpose with normal stress of formation.

(5) Model the fracture half-length and width propagation with time and compare with isothermal model.

An example of the thermal properties of the formation and fluid are shown in **Table 8** and input parameters for case study are shown in **Table 9** below.

	k (W/m° C)	C_p (J/Kg° C)	ρ (kg/m^3)	μ (Pa · s)
Formation	2.20	920.0	2640	Not Applied
Casing	43.33	418.7	8048.0	Not Applied
Fluid	0.586	4002.0	1000.0	0.0011

Table 8 Thermal properties for vertical hydraulic fracture analysis

Well Depth (m)	2000
Liquid Rate (m^3/s)	0.19
Well Perforation Depth (*m*)	2000
Formation Thickness (*m*)	30
Casing OD (m)	0.178
Liquid Injection Temperature ($^\circ$ C)	20
Surface Temperature ($^\circ$ C)	20
Geothermal Gradient ($^\circ$ C /*m*)	0.016
Formation Porosity	0.1
Poisson Ratio	0.25
Overburden Density (kg/m^3)	1.797
Young's Modulus (GPa)	30
Geomechanics Heterogeneity	2
Leak-off Coefficient ($m/min^{0.5}$)	0.004
Poroelastic Coefficient	0.2

Table 9 Input parameters for vertical hydraulic fracture analysis

The wellbore temperature profile at the bottomhole is simulated using the current model. The results are shown in **Figure 11.**

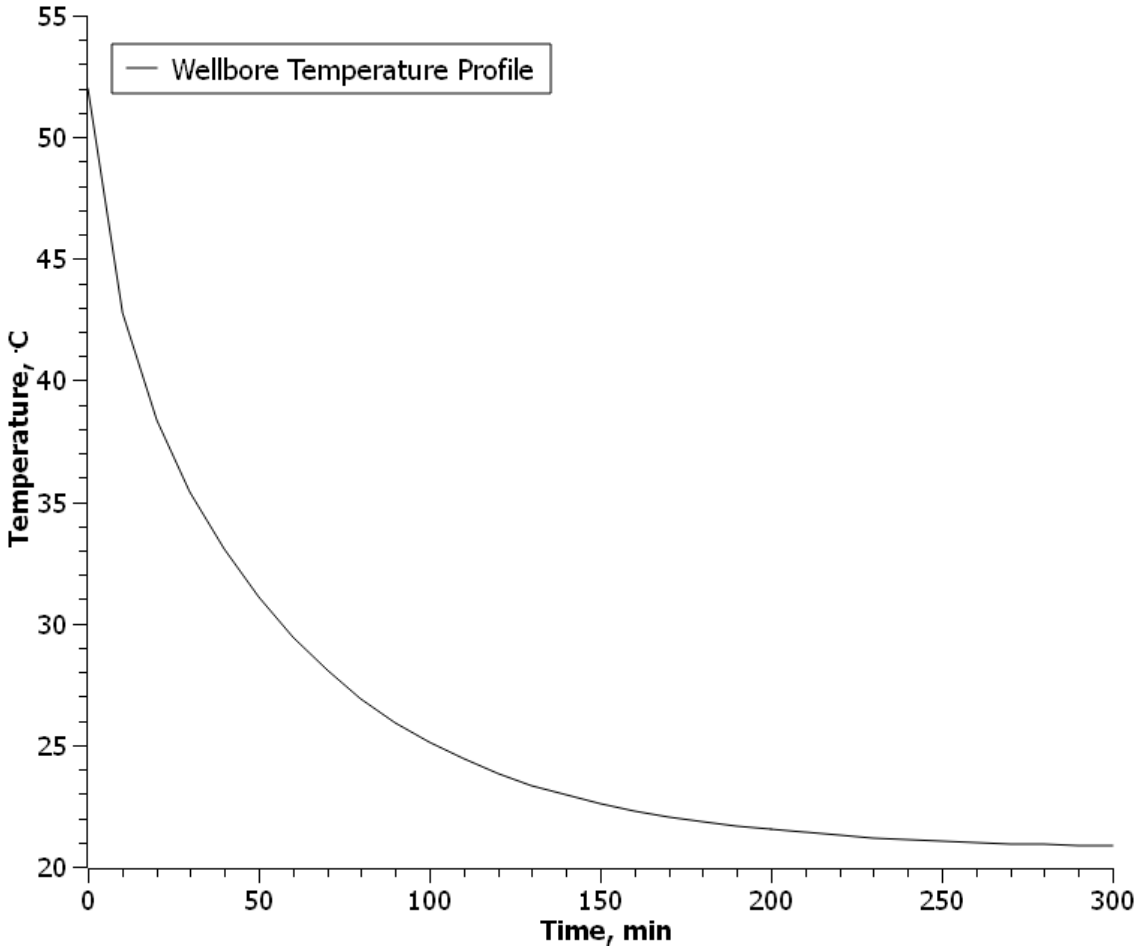

Figure 11 Bottomhole wellbore temperature profile, for vertical well hydraulic fracturing case study

Based on the temperature profile, calculations are then made for the viscosity change of brine with respect to pumping time. The results are shown in **Figure 12.**

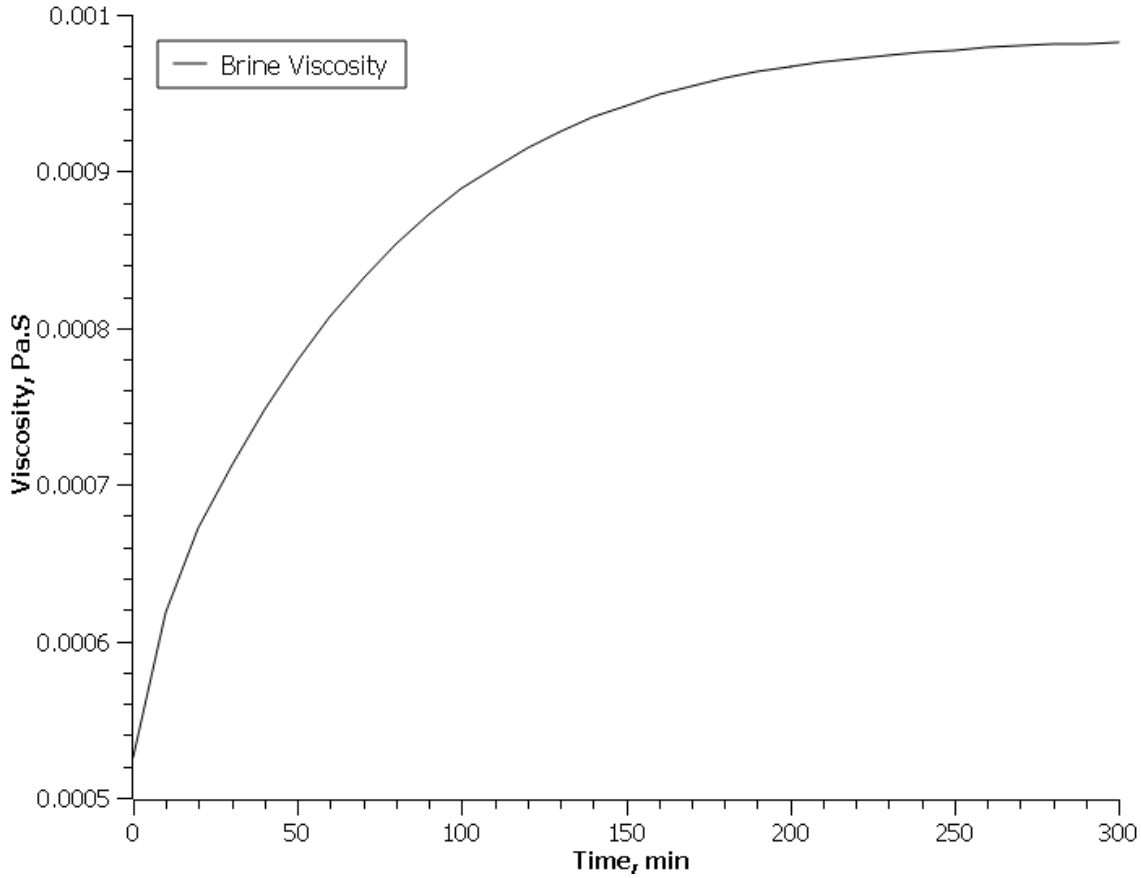

Figure 12 Brine viscosity change with time, for vertical well hydraulic fracturing case study

Overburden stress can be calculated using the overburden density using the equation:

$$S_v = \rho_{over} gh \tag{5.10}$$

Pore pressure can be calculated using the liquid density with the equation:

$$P_p = \rho gh \tag{5.11}$$

Stress state of this well is determined using the overburden stress and the geomechanics heterogeneity ratio. Based on

$$S_h = \frac{\nu}{1-\nu}\left(S_v - P_p\right) \tag{5.12}$$

Thus the static stress state of the formation are calculated and listed in the following **Table 10**.

Overburden Stress, MPa	26.89
Pore Pressure, MPa	15.24
Minimum Horizontal Stress, MPa	3.88
Maximum Horizontal Stress, MPa	7.76

Table 10 Static stress state of formation, for vertical well hydraulic fracturing case study

Thermal Stress is then calculated and superposed using Kirsch (Kirsch 1898) solution,

For the fracturing process, the thermal induced stress profile at perforation is shown in **Figure 13.**

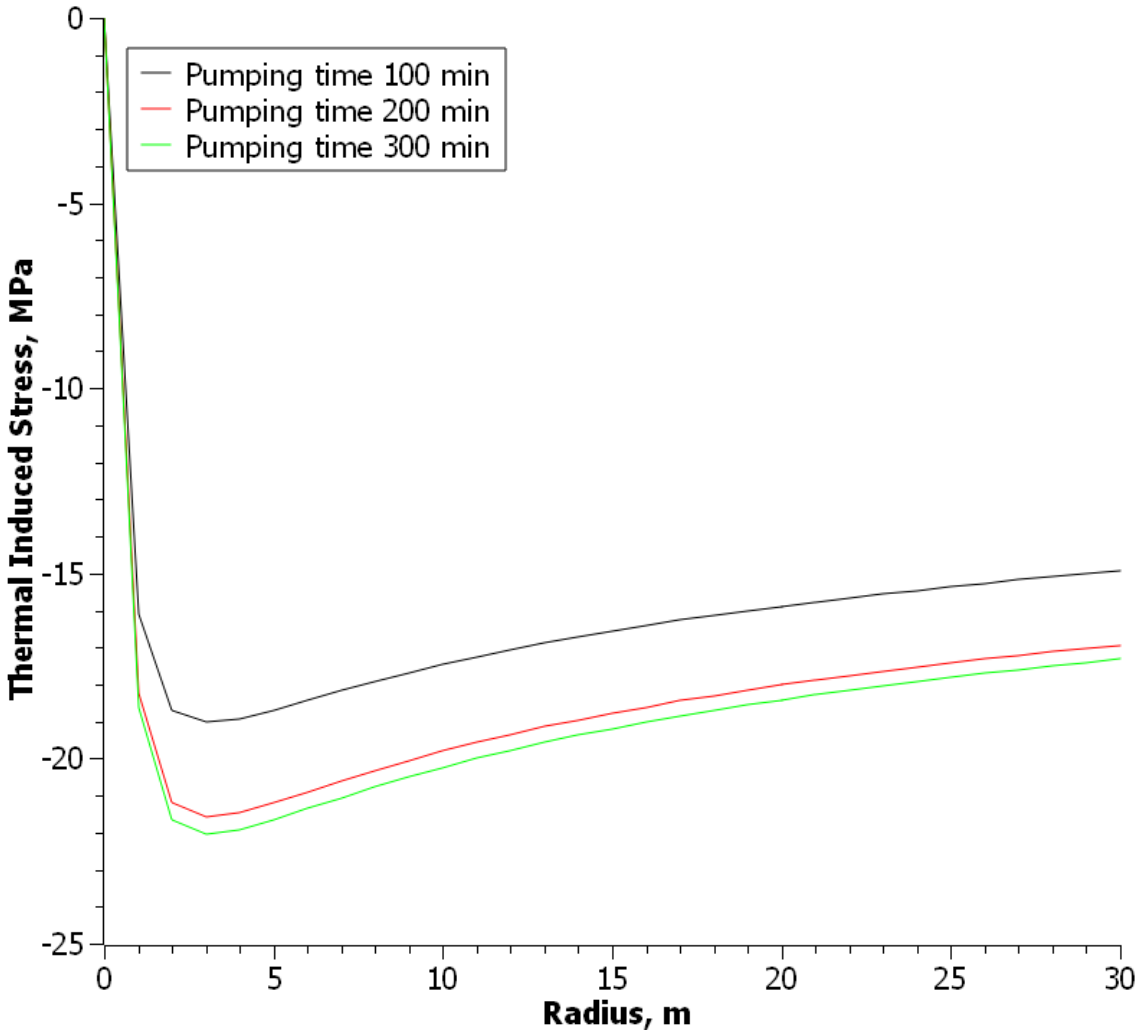

Figure 13 Thermal induced stress around a wellbore, for vertical well hydraulic fracturing case study

Coupling all these temperature impacts listed above, a PKN model (Perkins and Gonzalez 1984) is proposed to analyze the overall effect on fracture half-length and fracture with growth. The model description is shown in **Appendix C**.

Comparisons are made between a regular PKN fracture without considering temperature impact (Perkins and Kern 1961) and one case considering multiple temperature impacts listed above. The results are shown in **Figure 14** and **Figure 15.**

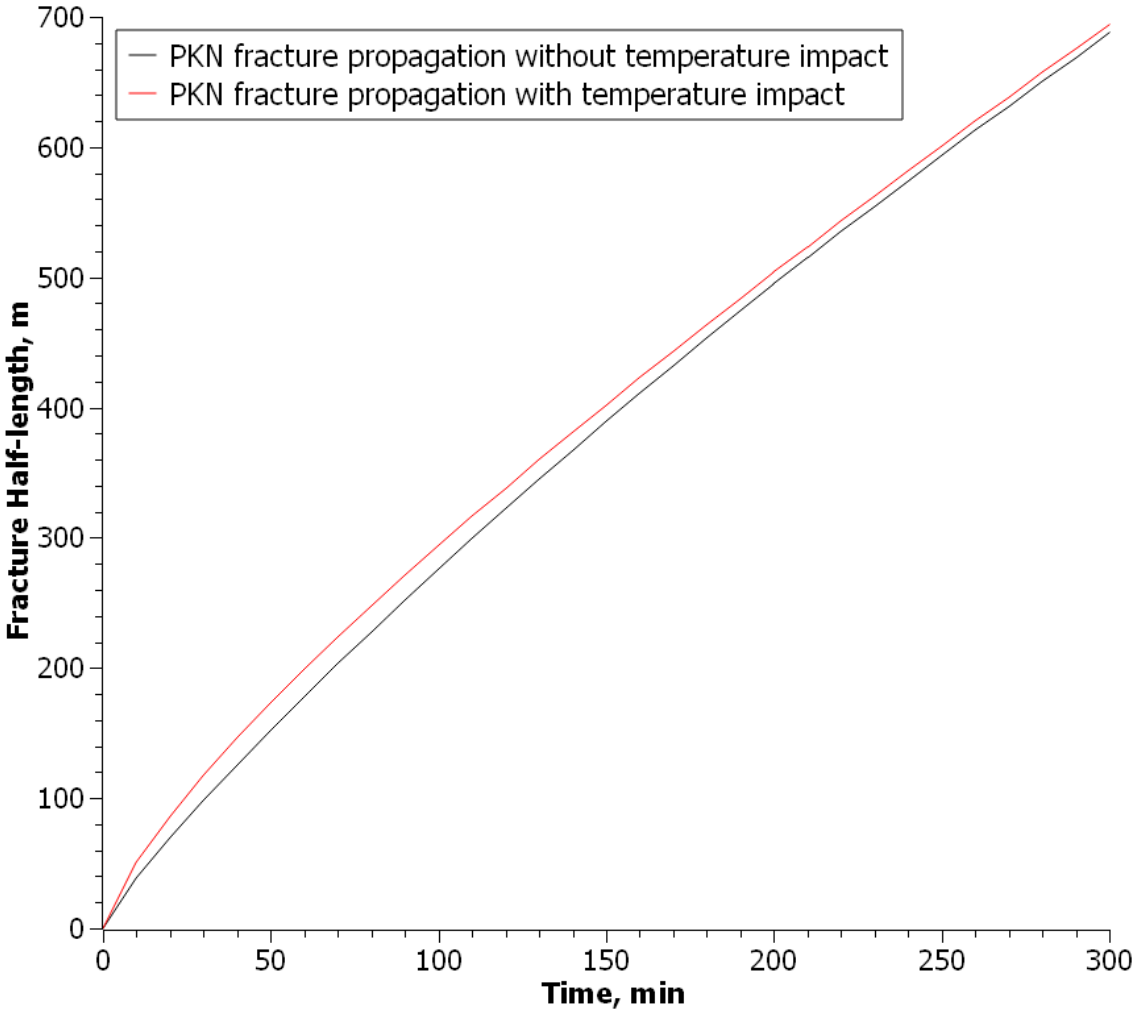

Figure 14 Hydraulic fracture half-length propagation with time, for vertical well hydraulic fracturing case study

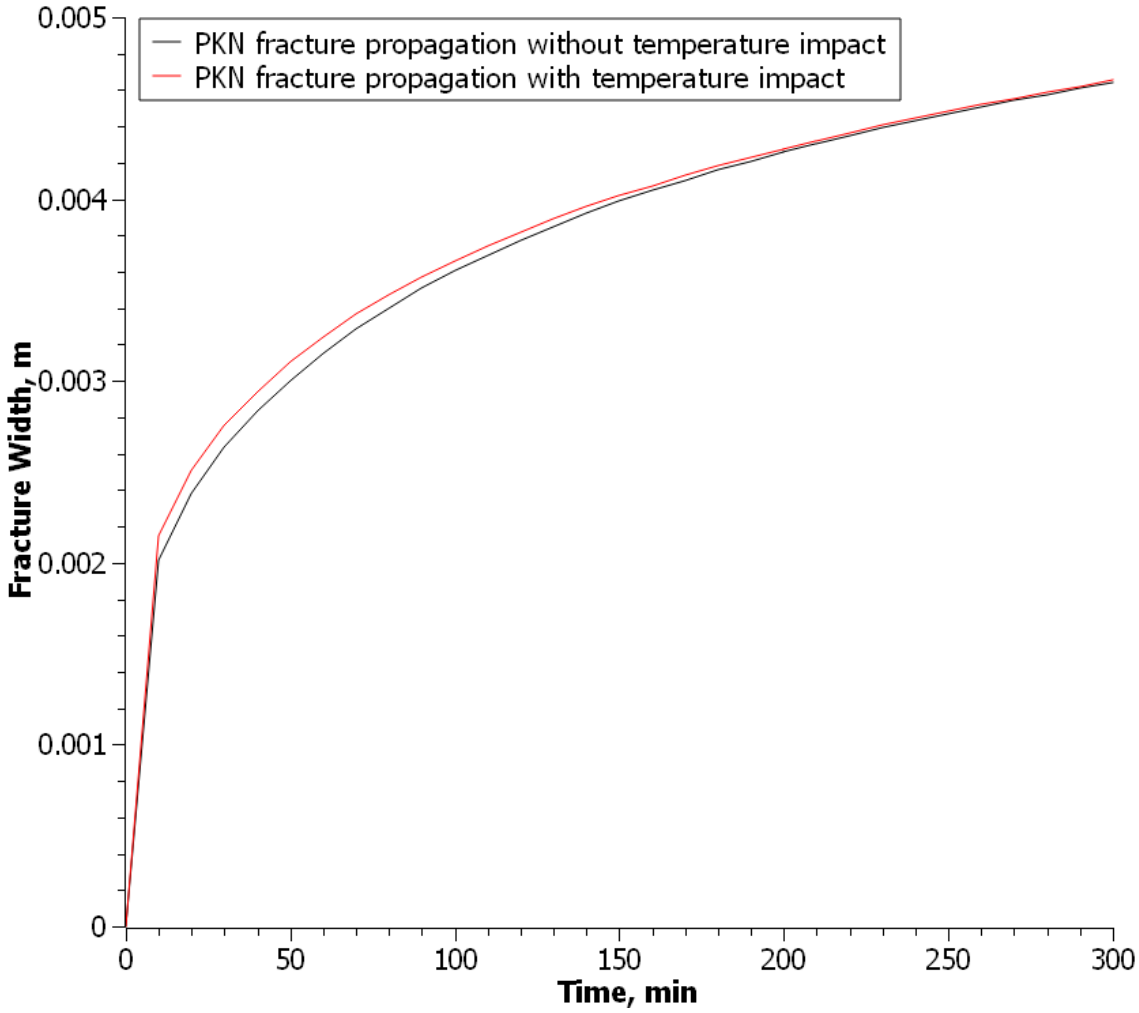

Figure 15 Hydraulic fracture width propagation with time, for vertical well hydraulic fracturing case study

Conclude from this case study and comparisons, for vertical hydraulic fractures, the transient temperature impacts tends to give out larger fracture half-length and slightly larger fracture width.

5.5 Temperature Impacts on Multistage Hydraulic Fracturing

Multistage hydraulic fracturing has been widely applied in horizontal well stimulation processes. When cold fracking fluid is transporting along the horizontal wellbore, the

fluid is heated and temperature along the horizontal piece tends to be different with respect to time and location.

To analyze the temperature impact on multistage hydraulic fracturing, it is necessary to study the temperature behavior in horizontal wellbore. This is done by coupling a vertical piece of simulation model and a revised horizontal piece together. The vertical piece calculates temperature at bottomhole with respect to time, $T_{bh}(t)$, and for the horizontal piece, the initial condition is changed to:

$$T_f(t, r=0)_{z=z_{\max}} = T_{bh}(t) \tag{5.13}$$

A case study is proposed to study the temperature profile of horizontal wellbore. The thermal properties of case study and input parameters are shown in **Table 11** and **Table 12**.

	k (W/m° C)	C_p (J/Kg° C)	ρ ($kg/$ m^3)	μ (Pa · s)
Formation	2.20	920.0	2640	Not Applied
Casing	43.33	418.7	8048.0	Not Applied
Fluid	0.586	4002.0	1000.0	0.0011

Table 11 Thermal properties of case study for multistage hydraulic fracturing

Well Depth (m)	2000
Liquid Rate (m^3/s)	0.19
Vertical Piece Depth (*m*)	2000
Horizontal Piece Length (*m*)	5000
Formation Thickness (*m*)	50
Casing OD (m)	0.178
Liquid Injection Temperature ($^\circ$ C)	20
Surface Temperature ($^\circ$ C)	20
Geothermal Gradient ($^\circ$ C /*m*)	0.016
Formation Porosity	0.1
Poisson Ratio	0.25
Overburden Density (kg/m^3)	1.797
Young's Modulus (GPa)	30
Geomechanics Heterogeneity	2
Leak-off Coefficient ($m/min^{0.5}$)	0.004
Poroelastic Coefficient	0.2

Table 12 Properties of case study for multistage hydraulic fracturing

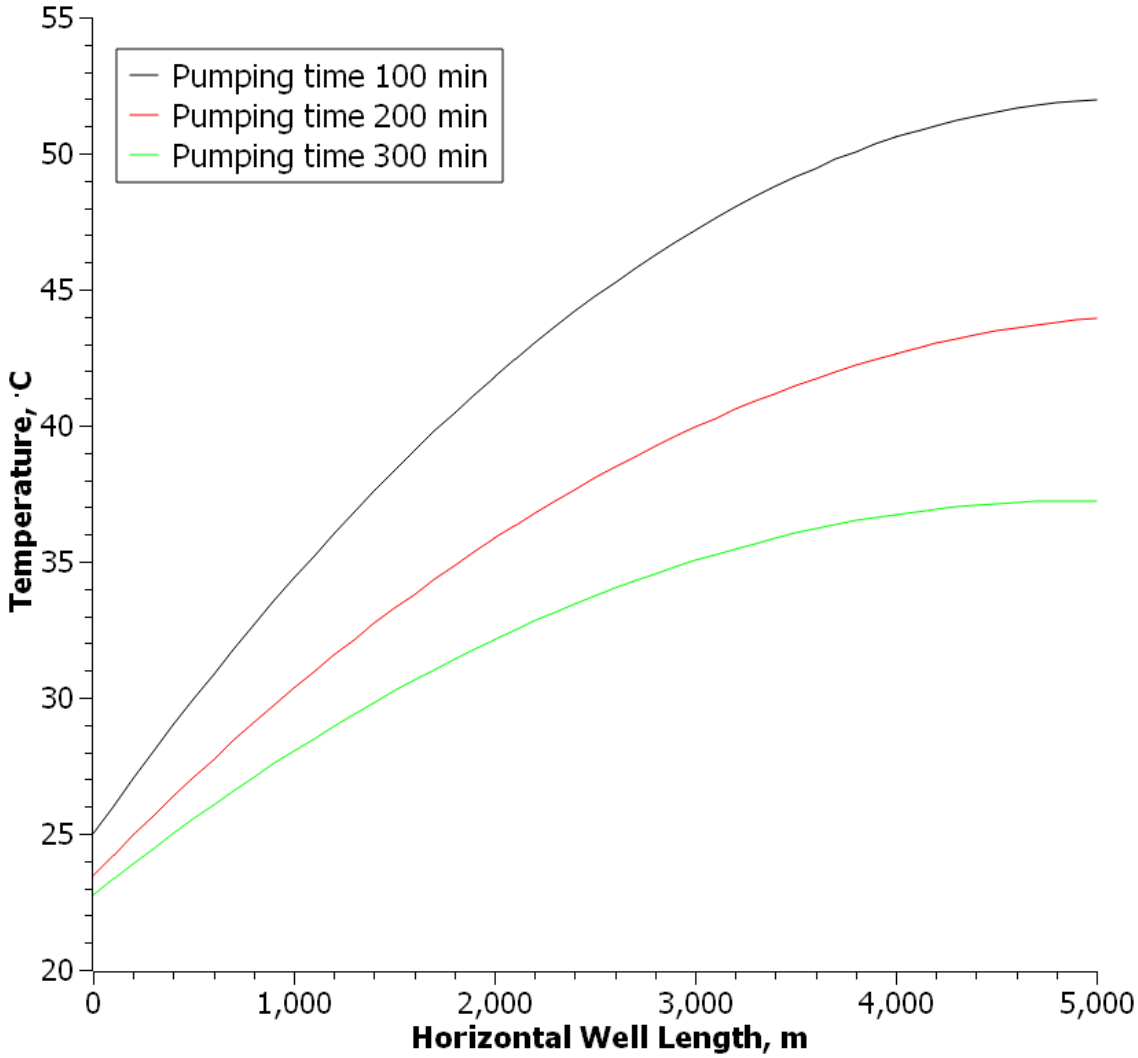

Figure 16 Temperature profile along horizontal wellbore, case study for multistage hydraulic fracturing

The temperature profile is shown in **Figure 16.** As time increases, the temperature at wellbore gradually decreases. This is reasoned from the cooling down of formation rock by fracking fluid.

A multistage hydraulic fracturing is performed at this horizontal piece. It is assumed that the PKN fracture fully penetrates the formation. 5 stages are applied during this process for every 60 minutes and every 1000m. The simulated fracture half-length with and without temperature impact are shown in **Figure 17.** This assures the conclusion

that fracture half-length increases with temperature impact. As the stage increases, the corresponding hydraulic fracture half-length decreases at the constant pumping rate.

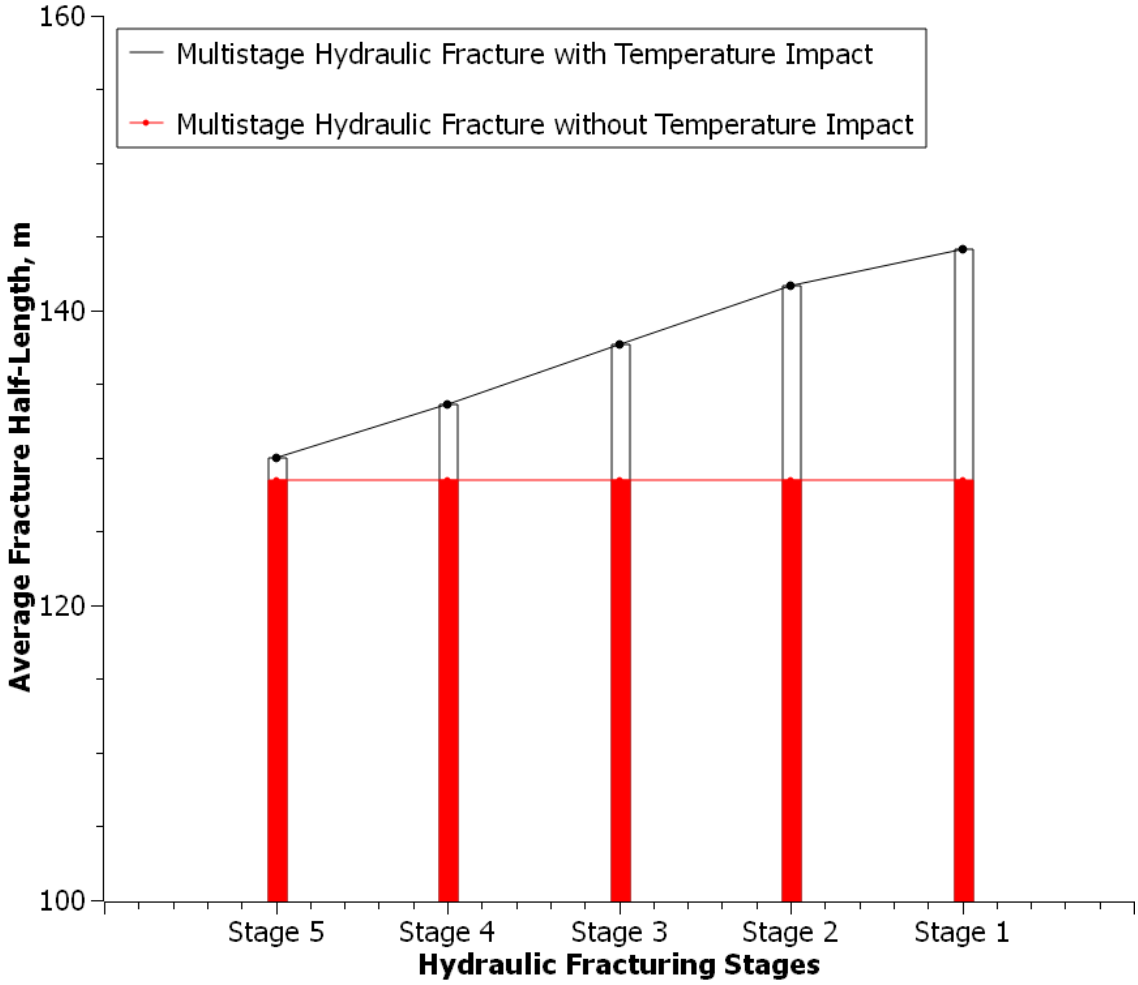

Figure 17 Multistage hydraulic fracture average half-length for every stage with temperature impact, case study for multistage hydraulic fracturing

Chapter 6: Conclusions and Future Steps

6.1 Conclusions

Based on the previous analysis and discussions, the following conclusions are drawn:

(1) An accurate model for transient temperature behavior in wellbore and its surrounding formations has been proposed. This model is based on mass balance and energy balance and solves the numerical problem using finite different method. This model calculates the temperature profile at any specific time and location.

(2) Validations on the model are conducted using Ramey's steady-state heat transmission model and Wu's transient model. The simulation results show good agreement with both validation cases.

(3) A case study is performed for a deepwater production well in the Gulf of Mexico. The temperature history profile is simulated and compared with gauge-measured data as a good approximation. The radial temperature distribution is then predicted, and some possible reasons for the difference between simulation and gauge data are discussed in the thesis.

(4) Studies are conducted on temperature impact of hydraulic fracturing. Both the horizontal propagating fracture in vertical well and multistage hydraulic fractures for horizontal wells are analyzed. By coupling the mechanisms, the temperature impacts tend to enlarge the fracture half-length as well as the fracture width. For multistage hydraulic fractures, the temperature behavior along horizontal wellbore tends to reduce the hydraulic fracture half-length with respect to different stages.

6.2 Future Steps

(1) Run case studies for hydraulic fracturing based on field data and compare the conclusions with current results.

(2) Collect more data to validate the transient temperature model under different scenarios.

(3) Couple the temperature impacts together with pressure for hydraulic fracturing. Compare the effectiveness of fracture propagation caused by pressure and temperature impacts.

(4) Conduct dimensionless analysis on temperature impacts of hydraulic fracturing and draw further conclusions.

References

Aboul-Seoud, A. and H. Moharam (1999). "A simple thermal conductivity-temperature correlation for undefined petroleum and coal liquid fractions." Chemical Engineering Research and Design **77**(3): 248-252.

American Petroleum, I. and R. Division of (1990). Design and operation of oil-water separators. Washington, D.C., American Petroleum Institute.

Beggs, H. D. and J. Robinson (1975). "Estimating the viscosity of crude oil systems." Journal of Petroleum technology **27**(09): 1,140-141,141.

Bird, R. B., et al. (2007). Transport phenomena, John Wiley & Sons.

Boone, T. and E. Detournay (1990). Response of a vertical hydraulic fracture intersecting a poroelastic formation bounded by semi-infinite impermeable elastic layers. International Journal of Rock Mechanics and Mining Sciences & Geomechanics Abstracts, Elsevier.

Bridgman, P. W. (1941). "Nature of thermodynamics."

Caslaw, H. and J. Jaeger (1986). Conduction of Heat in Solids, 2nd, Oxford, Clarendon Press.

Cassis, R., et al. (1985). "Specific heat capacities of bitumens and heavy oils, reservoir minerals, clays, dehydrated clays, asphaltenes, and cokes." Alberta Oil Sands Technology and Research Authority Journal of Research **1**(3): 163-173.

Cheng, A. and J. McLennan (1990). "A poroelastic PKN hydraulic fracture model based on an explicit moving mesh algorithm." Journal of Energy Resources Technology **112**: 225.

Dysart, G. and N. Whitsitt (1967). Fluid temperature in fractures. Fall Meeting of the Society of Petroleum Engineers of AIME, Society of Petroleum Engineers.

Economides, M. (1987). "Applied geothermics."

Edwardson, M., et al. (1962). "Calculation of formation temperature disturbances caused by mud circulation." Journal of Petroleum technology **14**(04): 416-426.

Ershaghi, I., et al. (1983). "Estimation of geothermal brine viscosity." Journal of Petroleum technology **35**(03): 621-628.

Farris, R. F. (1941). A practical evaluation of cements for oil wells. Drilling and Production Practice, American Petroleum Institute.

Gnielinski, V. (1975). "New equations for heat and mass transfer in the turbulent flow in pipes and channels." NASA STI/recon technical report A **75**: 8-16.

Gogoi, R. (1986). Thermal stresses around an uncased production well, Louisiana Tech Univ., Ruston (USA).

Hagoort, J. (2004). "Ramey's wellbore heat transmission revisited." SPE journal **9**(04): 465-474.

Hasan, A. R., et al. (2002). Fluid flow and heat transfer in wellbores, Society of Petroleum Engineers Richardson, Texas.

Haynes, W. M. (2014). CRC handbook of chemistry and physics, CRC press.

Horai, K. i. (1971). "Thermal conductivity of rock‐forming minerals." Journal of Geophysical Research **76**(5): 1278-1308.

Horne, R. and K. Shinohara (1979). "Wellbore heat loss in production and injection wells." Journal of Petroleum technology **31**(01): 116-118.

Izgec, B. (2008). Transient fluid and heat flow modeling in coupled wellbore/reservoir systems, Texas A&M University.

Kestin, J., et al. (1981). "Tables of the dynamic and kinematic viscosity of aqueous NaCl solutions in the temperature range 20–150 °C and the pressure range 0.1–35 MPa." Journal of Physical and Chemical Reference Data **10**(1): 71-88.

Kirsch, G. (1898). Die Theorie der Elastizität und die Bedürfnisse der Festigkeitslehre, Springer.

Kutasov, I. (1989). "Application of the Horner method for a well produced at a constant bottomhole pressure." SPE Formation Evaluation **4**(01): 90-92.

Lesem, L. B., et al. (1957). "A method of calculating the distribution of temperature in flowing gas wells."

McAdams, W. H. (1958). "Heat transmission."

Meyer, B. R. (1989). "Heat transfer in hydraulic fracturing." SPE production engineering **4**(04): 423-429.

Miller, C. W. (1980). "Wellbore storage effects in geothermal wells." Society of Petroleum Engineers Journal **20**(06): 555-566.

Newson, T. and P. Brunning (2004). "Thermal conductivity of deepwater offshore sediments." International Journal of Offshore and Polar Engineering **14**(04).

Nordgren, R. (1972). "Propagation of a vertical hydraulic fracture." Society of Petroleum Engineers Journal **12**(04): 306-314.

Pátek, J., et al. (2009). "Reference correlations for thermophysical properties of liquid water at 0.1 MPa." Journal of Physical and Chemical Reference Data **38**(1): 21-29.

Perkins, T. and J. Gonzalez (1984). "Changes in earth stresses around a wellbore caused by radially symmetrical pressure and temperature gradients." Society of Petroleum Engineers Journal **24**(02): 129-140.

Perkins, T. and L. Kern (1961). "Widths of hydraulic fractures." Journal of Petroleum technology **13**(09): 937-949.

Prats, M. (1982). "Thermal recovery."

RAMEY JR, H. (1962). "Wellbore heat transmission."

Ramires, M. L., et al. (1995). "Standard reference data for the thermal conductivity of water." Journal of Physical and Chemical Reference Data **24**(3): 1377-1381.

Riazi, M. R. and A. Faghri (1985). "Thermal conductivity of liquid and vapor hydrocarbon systems: pentanes and heavier at low pressures." Ind. Eng. Chem. Process Des. Dev.;(United States) **24**(2).

Robertson, E. C. (1988). Thermal properties of rocks, US Geological Survey.

Sagar, R., et al. (1991). "Predicting temperature profiles in a flowing well." SPE production engineering **6**(04): 441-448.

Santoyo-Gutierrez, E. R. (1997). Transient numerical simulation of heat transfer processes during drilling of geothermal wells, University of Salford.

Sharma, Y., et al. (1989). "Simulation of downhole heater phenomena in the production of wellbore fluids." SPE production engineering **4**(03): 309-312.

Shiu, K. and H. Beggs (1980). "Predicting temperatures in flowing oil wells." Journal of Energy Resources Technology **102**(1): 2-11.

Sieder, E. N. and G. E. Tate (1936). "Heat transfer and pressure drop of liquids in tubes." Industrial & Engineering Chemistry **28**(12): 1429-1435.

Somerton, W. H. (1958). "Some thermal characteristics of porous rocks."

Vazquez, M. and H. D. Beggs (1980). "Correlations for fluid physical property prediction." Journal of Petroleum technology **32**(06): 968-970.

Vosteen, H.-D. and R. Schellschmidt (2003). "Influence of temperature on thermal conductivity, thermal capacity and thermal diffusivity for different types of rock." Physics and Chemistry of the Earth, Parts A/B/C **28**(9): 499-509.

Waples, D. W. and J. S. Waples (2004). "A review and evaluation of specific heat capacities of rocks, minerals, and subsurface fluids. Part 1: Minerals and nonporous rocks." Natural resources research **13**(2): 97-122.

Waples, D. W. and J. S. Waples (2004). "A review and evaluation of specific heat capacities of rocks, minerals, and subsurface fluids. Part 2: fluids and porous rocks." Natural resources research **13**(2): 123-130.

Wheeler, J. (1969). Analytical calculations for heat transfer from fractures. SPE Improved Oil Recovery Symposium, Society of Petroleum Engineers.

Whitsitt, N. and G. Dysart (1970). "The effect of temperature on stimulation design." Journal of Petroleum technology **22**(04): 493-502.

Wilke, C. (1950). "A viscosity equation for gas mixtures." The journal of chemical physics **18**(4): 517-519.

Willhite, G. P. (1967). "Over-all heat transfer coefficients in steam and hot water injection wells." Journal of Petroleum technology **19**(05): 607-615.

Wu, X., et al. (2015). "A semi-analytical solution to the transient temperature behavior along the vertical wellbore after well shut-in." Journal of Petroleum Science and Engineering **131**: 122-130.

Wu, Y.-S. and K. Pruess (1990). "An Analytical Solution for Wellbore Heat Transmission in Layered Formations (includes associated papers 23410 and 23411)." SPE Reservoir Engineering **5**(04): 531-538.

Xiang, J. (2011). A PKN Hydraulic Fracture Model Study and Formation Permeability Determination, Texas A&M University.

Zoth, G. and R. Haenel (1988). Appendix. Handbook of Terrestrial Heat-Flow Density Determination, Springer**:** 449-468.

Appendix A: Property Variations and Temperature Dependence

The rock and fluid properties vary when temperature changes. In this thesis, several correlations are applied to calculate the temperature dependence of rock and fluid properties. This appendix discusses this dependency and correlations used for estimating different rock and fluid properties.

A.1 Rock Properties

Due to the complexity of rock (lithology, porosity, fluid composition), there is no analytical method to calculate the rock property change for all types. However, some empirical correlations based on sample studies and regressions can be used to estimate the thermal properties of rock.

A.1.1 Thermal Conductivity

Thermal conductivity for formation rock is a function of its temperature, dry density, moisture content, mineralogy, particle size, shape and arrangement (Newson and Brunning 2004). Numerous studies have been made to study the thermal conductivity of formation rock. One made by Horai (Horai 1971) has measured the thermal conductivity of multiple rock-forming minerals, shown in **Table 13**.

Material	Thermal conductivity (mcal/cm s ° C)
Quartz	18.37
Micas	5.96
Feldspars	6.21
Calcite	8.58
Magnetite	12.18
Pyroxene	9.13
Amphibole	9.47

Table 13 Thermal conductivity of common rock-forming minerals (Horai 1971)

The method used to calculate the temperature dependency of thermal conductivity is based on Zoth and Haenel (Zoth and Haenel 1988). For different rock types,

$$k(T) = \frac{705}{350 + T} + 0.64 \tag{7.1}$$

Where T is in $^{\circ}C$ and k is in $W/\left(m \cdot {}^{\circ}K\right)$.

A.1.2 Specific Heat Capacity

Specific heat capacity is the extensive property of a system. It is defined as the ratio of heat added to (or removed from) an object to the resulting temperature change at per unit mass. In the field of petroleum engineering, the rock and fluids have different specific heat capacity due to differences of their materials. This property is affected by composition, porosity, water content, pressure and temperature (Robertson 1988).

W.Waples and S. Waples (Waples and Waples 2004) has studied the minerology impacts on heat capacity. According to his list, the specific heat capacity at standard condition for some common rock forming minerals is shown in **Table 14**.

Material	Specific Heat Capacity (J/kg° K)
Quartz	740
Micas	770
Feldspars	685
Calcite	815
Magnetite	586
Pyroxene	752
Amphibole	749

Table 14 Specific heat capacity of common rock-forming minerals (Waples and Waples 2004)

Somerton (Somerton 1958) has studied the specific heat capacity of different rock types under varied temperature. His work is shown in **Figure 18.**

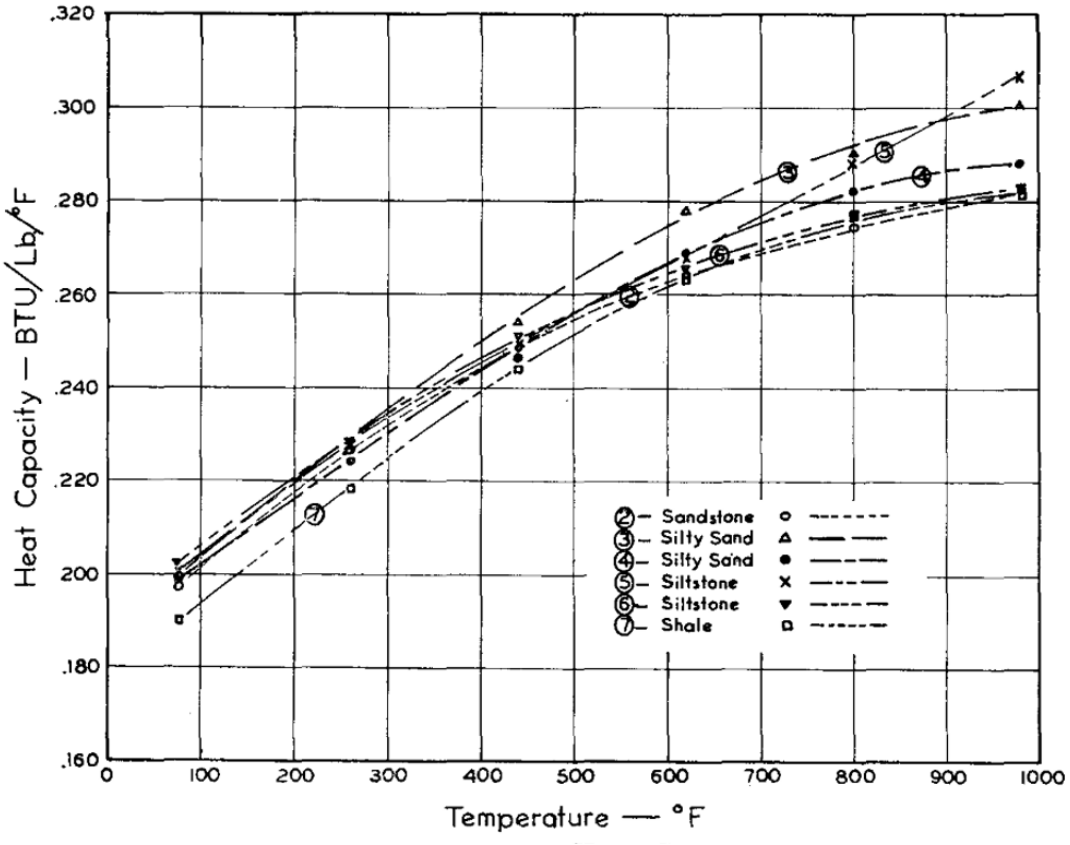

Figure 18 Specific heat capacity of rock at different temperatures (Somerton 1958)

The method used to calculate the temperature dependency of specific heat conductivity is based on Vosteen and Schellschmidt (Vosteen and Schellschmidt 2003). The correlation graph of rock is shown in **Figure 19.**

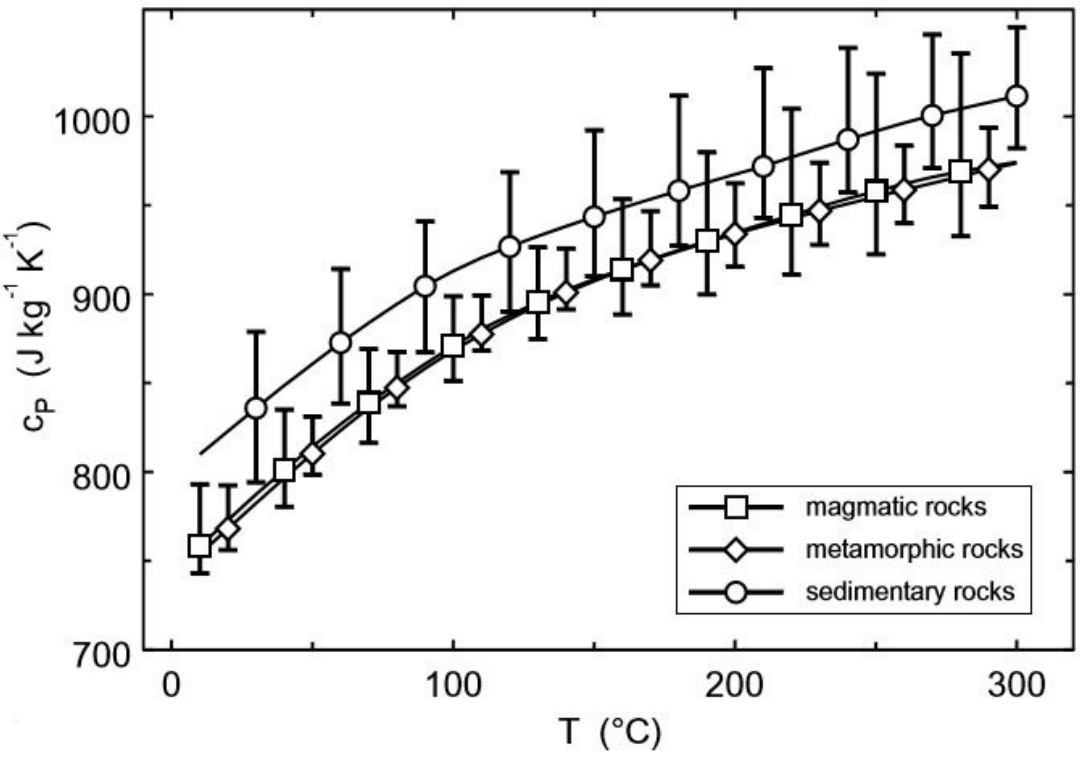

Figure 19 Correlation of rock specific heat capacity with temperature (Vosteen and Schellschmidt 2003)

A.2 Fluids

In this thesis, the most common fluids are oil and water. These fluids have different properties, and different correlations apply to solve for the temperature dependent properties.

A.2.1 Thermal Conductivity

Many researches have been done to study the thermal conductivity of fluids. For liquids, the most theoretical and semi-empirical method is developed by P.W. Bridgman (Bridgman 1941). Bridgman's equation calculates the thermal conductivity of liquids by using:

$$k = 3.0\left(\frac{N}{V}\right)^{\frac{2}{3}} K_B v_s \tag{7.2}$$

Where k represents the thermal conductivity in $W/\left(m\cdot{}^{\circ}K\right)$, the N and K_B are Avogadro's number and Boltzmann's constant, respectively. V is the molar volume, and v_s is the speed of sound through the fluid of interest.

For fluids in gas phase, CRC Handbook (Haynes 2014) has provided values of thermal conductivity at standard condition for some common pure gas in the field of petroleum engineering. These are listed in **Table 15**.

Gas	Thermal conductivity (W/m° K)
Methane	0.033
Ethane	0.017
Propane	0.017
Air	0.025
Carbon dioxide	0.015
Nitrogen	0.024

Table 15 Thermal conductivity of some common gases (Haynes 2014)

And for gas mixtures, Wilke's Rule (Wilke 1950) can be applied to estimate the thermal conductivity,

$$k_{mix} = \sum_{i=1}^{n} \frac{x_i k_i}{\sum_{j=1}^{n} x_j \Phi_{ij}} \tag{7.3}$$

where x_i is the mole fraction of its ith component and Φ_{ij} is the scaling factor.

The thermal conductivity of water is calculated using the NIST correlation (Ramires, Nieto de Castro et al. 1995).

$$k(T)=\left(-1.48445+4.12292\left(\frac{T}{298.15}\right)-1.63866\left(\frac{T}{298.15}\right)^{2}\right)\cdot k(298.15) \quad (7.4)$$

Where T is in $^{\circ}K$ and k is in $W/\left(m\cdot{}^{\circ}K\right)$.

The correlation for hydrocarbon mixture is based on the combination of Riazi (Riazi and Faghri 1985) and Aboul-Seoud (Aboul-Seoud and Moharam 1999).

$$k(T)=0.0655-0.00005T+\left(1.3855-0.00197T\right)/MW^{0.5} \quad (7.5)$$

Where the molecular weight of undefined hydrocarbon mixture MW can be calculated using Raizi:

$$MW=\sqrt{\frac{1.11}{k_L\left(T_{ref}\right)}} \quad (7.6)$$

where k_L is the thermal conductivity at a reference temperature.

A.2.2 Specific Heat Capacity

Water has higher specific heat capacity than other fluids. Patek (Pátek, Hrubý et al. 2009) has studied the specific heat capacity of water using a method of sound velocity at different temperature, shown in **Table 16**.

Temperature $^{\circ}K$	Specific Heat Capacity (J/kg$^{\circ}$ K)
260	4300.14772
298.15	4181.44618
375	4217.74697

Table 16 Water specific heat capacity at different temperature (Pátek, Hrubý et al. 2009)

W.Waples and S. Waples (Waples and Waples 2004) at another research has studied the specific heat capacity of oil at different specific gravity and varied temperature. According to their work (**Figure 20**), as the oil density increases, its heat capacity also increases.

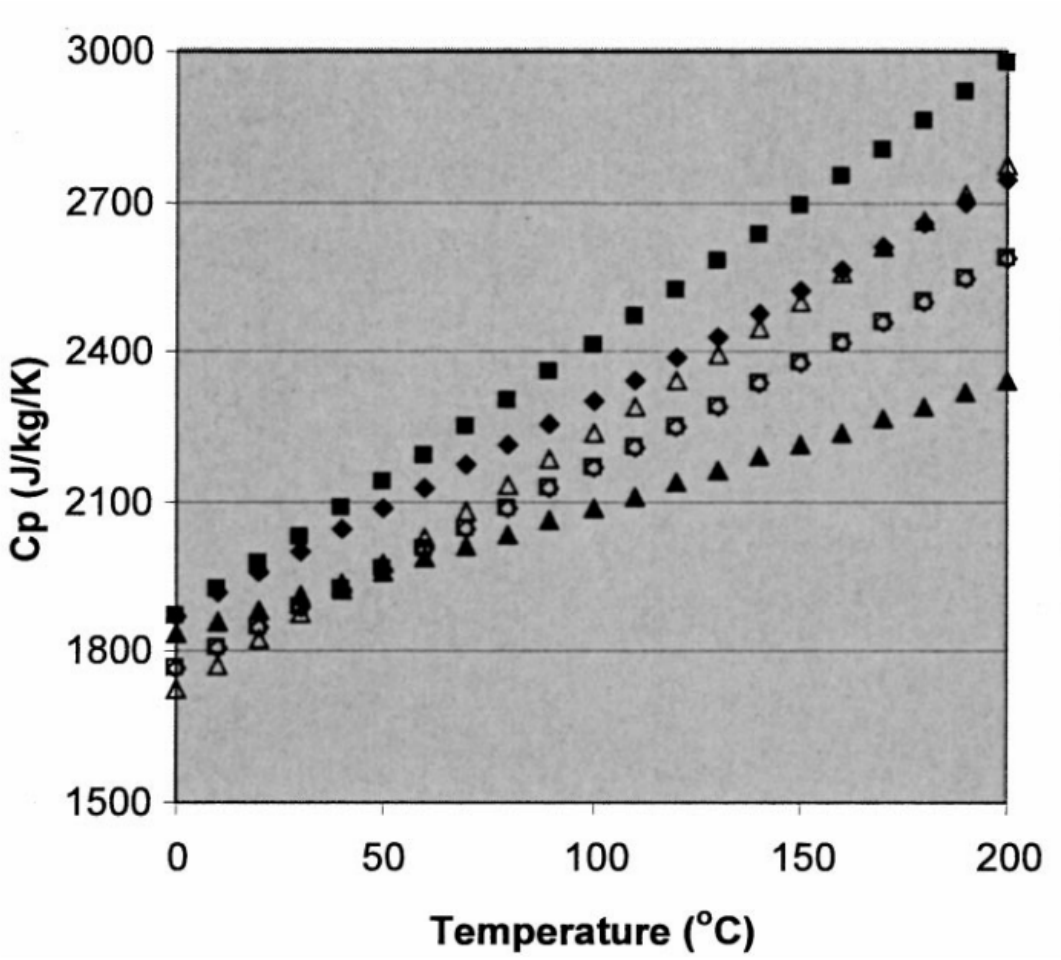

Figure 20 Specific heat capacity of oil samples vs. temperature, ranging from 25 API to 45 (Waples and Waples 2004)

The specific heat capacity of water is calculated using Cassis (Cassis, Fuller et al. 1985) correlation. For pure water,

$$C_{pw} = 4.182 - 1.5\times10^{-4}T + 3.44\times10^{-7}T^2 + 4.26\times10^{-8}T^3 \qquad (7.7)$$

Where T is in $^{\circ}C$ and C_{pw} is in $J/\left(mol\cdot{}^{\circ}K\right)$.

The specific heat capacity for hydrocarbon is calculated using the API (American Petroleum and Division of 1990) correlation.

$$C_{po} = \left(-1.39\times10^{-6}T + 1.847\times10^{-3}\right)\cdot {}^{\circ}API + 6.312\times10^{-4}T + 0.352 \qquad (7.8)$$

Where T is in ${}^{\circ}F$, ${}^{\circ}API$ is the API gravity of oil, and C_{pw} is in $\text{Btu}/\left(lb\cdot {}^{\circ}F\right)$.

A.2.3 Viscosity

The viscosity of a fluid is a measure of its resistance to gradual deformation by shear or tensile stress. It is a combination of its temperature, pressure, composition and concentration.

For water or brine in petroleum industry, the function of fluid viscosity is dependent of its salinity, pressure and temperature. Ershaghi (Ershaghi, Abdassah et al. 1983) studied the brine viscosity at geothermal condition. According to his study, the viscosity of brine decreases as temperature increases and water salinity decreases, shown in **Figure 21.**

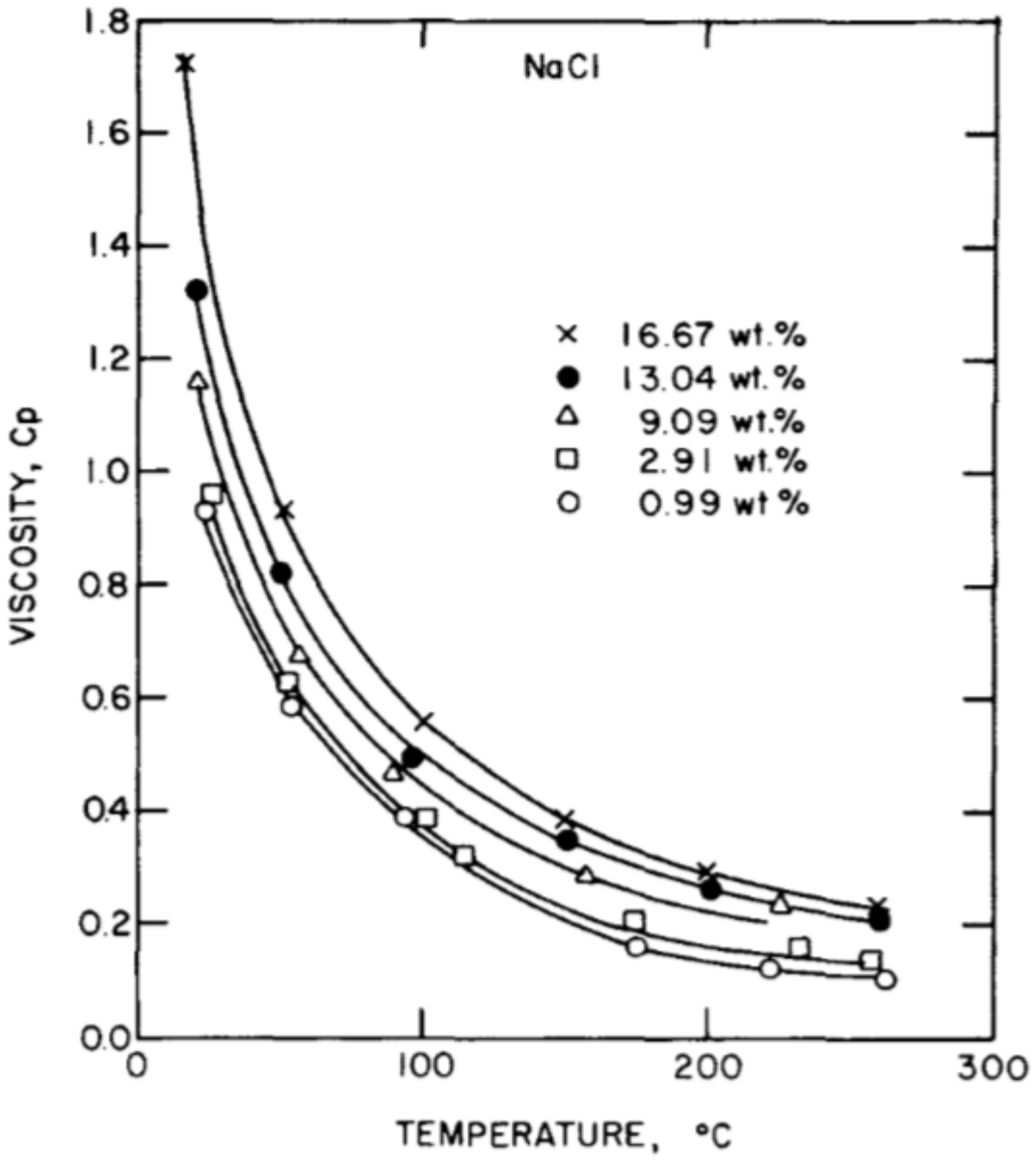

Figure 21 Brine viscosity vs. temperature (Ershaghi, Abdassah et al. 1983)

Oil viscosity is more complexed. It is affected by its gas-oil solution ratio as well as hydrocarbon compositions. Below the bubble point pressure, the effect of solution gas decreases oil viscosity. When pressure raises above the bubble point, viscosity increases almost linearly with pressure (Vazquez and Beggs 1980).

The method used to calculate the water viscosity is developed by Kestin et al. (Kestin, Khalifa et al. 1981). Detailed calculation steps are listed in Chapter 5.

$$\mu(p,T,m) = \mu^0(T,m)\left[1+\beta(T,m)\cdot p\right] \tag{7.9}$$

Where μ^0 is the hypothetical zero-pressure viscosity, and β is pressure coefficient.

The oil viscosity calculation is based on Beggs and Robinson (Beggs and Robinson 1975).

$$\mu_{od} = 10^x - 1 \tag{7.10}$$

Where

$$x = yT^{-1.163} \tag{7.11}$$

$$y = 10^z \tag{7.12}$$

$$z = 3.0324 - 0.02023G \tag{7.13}$$

Appendix B: Determination of Convective Heat Transfer Coefficient

The heat convection between pipe wall and liquid film is analyzed using convective heat transfer equation with respect to convective heat transfer coefficient, *h*. This coefficient is calculated based on Nusselt number, Nu, which was discussed by Santoyo-Gutierrez (Santoyo-Gutierrez 1997).

$$Nu = \frac{h}{k} D_h \tag{8.1}$$

For laminar flow regime, the Nusselt number for fluid in tubing and annulus are calculated separately. For the tubing region, an analytical solution gives that

$$Nu = 4.364 \tag{8.2}$$

as a constant, and *h* can be calculated directly from (8.1). For the annulus region, Sieder and Tate (Sieder and Tate 1936) has provided with a correlation, which is shown in (8.3)

$$Nu = 1.86 \left(\frac{\mathrm{Re} \cdot \mathrm{Pr} \cdot D}{L} \right)^{\frac{1}{3}} \left(\frac{\mu_b}{\mu_s} \right)^{0.14} \tag{8.3}$$

For transitional and turbulent flow, Nu is a function of several different parameters. Gnielinski (Gnielinski 1975) has provided a correlation to estimate the Nusselt number for transitional flow, which is shown in (8.4).

$$Nu = \frac{\left(\frac{f}{8} \right) (\mathrm{Re} - 1000) \mathrm{Pr}}{1 + 12.7 \left(\frac{f}{8} \right)^{0.5} \left(\mathrm{Pr}^{\frac{2}{3}} - 1 \right)} \tag{8.4}$$

Where f is the friction factor,

$$f = \left(0.79 \ln(\mathrm{Re}) - 1.64 \right)^{-2} \tag{8.5}$$

Pr is the Prandtl number, calculated by:

$$\mathrm{Pr} = \frac{\mu}{k} C_p \tag{8.6}$$

And *Re* is the Reynolds number,

$$\mathrm{Re} = \frac{\rho v D}{\mu} \tag{8.7}$$

Appendix C: Fracture Propagation Model

A PKN fracture model is used to couple all the temperature-influenced parameters listed in Chapter 5 together for analyzing the overall temperature impact on hydraulic fracturing. The detailed description of this model is shown in below.

For a propagating fracture, the fracture width can be described as a function of (Xiang 2011):

$$w = w_e + w_p \tag{9.1}$$

Where w_e is the fracture width change controlled by net stress effect and w_p is controlled by net pressure effect.

The net stress effect is approximated as being purely elastic. Cheng and Mclennan (Cheng and McLennan 1990) presented a description about this effect as:

$$w_e = M_c \left(p_f - \sigma_{\min,corr} \right) \tag{9.2}$$

Where M_c is the fracture compliance, described by

$$M_c = \frac{\pi (1-\nu) H}{4G} \tag{9.3}$$

p_f is the fracture pressure. $\sigma_{\min,corr}$ is the minimum corresponding horizontal stress, which is the superposition of minimum horizontal stress σ_h and the thermal induced stress σ_{th} . In a radial coordinate system,

$$\sigma_{\theta \min,corr} = \sigma_{\theta,h} + \sigma_{\theta,th} \tag{9.4}$$

The net pressure poroelastic effect can be described by (Boone and Detournay 1990):

$$w_p = -2\eta \Delta p M_c f\left(t^*\right) \tag{9.5}$$

η is the poroelastic coefficient. Its theoretical value is 0.5. Δp is the fracture pressure minus the pore pressure. $f\left(t^*\right)$ is an evolutional function which varies between 0 and 1. The t^* denotes as dimensionless fracture surface exposure time, defined as:

$$t^* = \frac{4ct}{H^2} \tag{9.6}$$

H is the fracture height. c is a diffusivity coefficient, defined by:

$$c = \frac{k}{\phi \mu C_p} \tag{9.7}$$

Boone and Detournay (Boone and Detournay 1990) gave out an expression for $f\left(t^*\right)$ as:

$$f\left(t^*\right) = \frac{4}{\pi}\int_0^\infty erfc\left(\frac{y}{2\sqrt{t^*}}\right) g\left(y\right) dy \tag{9.8}$$

And

$$g\left(y\right) = 1 - \sqrt{\frac{y}{2}}\sqrt{\sqrt{4+y^2}-y} \tag{9.9}$$

Substituting these equations into (9.1) gives a correlation fracture width. This equation is then combined with Carter's (Carter 1957) solution for the fracture half-length with time:

$$L\left(t\right) = \frac{Q\left(t\right)w}{8\pi H C_L^2}\left(e^{S^2} erfc\left(S\right) + \frac{2}{\sqrt{\pi}}S - 1\right) \tag{9.10}$$

Where

$$S = \frac{2C_L\sqrt{\pi t}}{w} \tag{9.11}$$

This solved fracture half-length is then coupled with Perkins and Kern (Perkins and Kern 1961) width equation iteratively, until a consistent solution is found.

$$w(x) = 3\left[\frac{\mu Q(t)(L-x)(1-\nu^2)}{E}\right] \tag{9.12}$$

While the temperature impact on hydraulic fracturing is not being considered, Nordgren (Nordgren 1972) proposed an approximation for the previous estimations of fracture height and width with time, which is used in the case study for comparison:

$$t_D = \left[\frac{64C_L^5 EH}{\pi^3 \mu Q^2(t)(1-\nu^2)}\right]^{\frac{2}{3}} t \tag{9.13}$$

$$L_D(t_D) = 1.56 t_D^{\frac{4}{5}} \tag{9.14}$$

$$w_D(t_D) = 1.09 t_D^{\frac{1}{5}} \tag{9.15}$$

And

$$L_D = \frac{1}{4}\left[\frac{G}{(1-\nu)\mu Q(t)}\right]^{\frac{1}{3}} L \tag{9.16}$$

$$w_D = \frac{1}{4}\left[\frac{G}{(1-\nu)\mu Q(t)}\right]^{\frac{1}{3}} w \tag{9.17}$$

Appendix D: Nomenclature

Normal Nomenclature

A	=	Area, m^2
A_{pipe}	=	Pipe inner area, m^2
C_L	=	Leak-off coefficient, $m/min^{0.5}$
C_p	=	Heat capacity, $J/(Kg^{\circ} C)$
c	=	Diffusivity coefficient, m^2/s
D_h	=	Hydraulic diameter, m
E	=	Young's modulus, MPa
f	=	Friction factor
$f(t)$	=	Time function of Ramey's model
$f(t^*)$	=	Evolutional function
h	=	Convective heat transfer coefficient, $W/(m^{2\ \circ} C)$
G	=	Shear modulus, MPa
g	=	Gravitational acceleration, m/s^2
k_r	=	Thermal conductivity in radial direction, $W/(m^{\circ} C)$
k_z	=	Thermal conductivity in vertical direction, $W/(m^{\circ} C)$
L	=	Fracture half-length, m
L_D	=	Dimensionless fracture half-length
M_c	=	Fracture compliance, m/MPa
Nu	=	Nusselt number

Pr	=	Prandtl Number
p	=	Pressure, Pa
P_p	=	Pore pressure, MPa
$Q(t)$	=	Volumetric fluid rate, m^3/d
q	=	Heat flux rate due to molecular transport, J/s
q_r	=	Heat flux in radial direction, J/s
q_z	=	Heat flux in vertical direction, J/s
Re	=	Reynolds numbe
R_D	=	Dimensionless radius of thermal influence
r_D	=	Dimensionless radial distance
S_h	=	Minimum horizontal Stress, MPa
S_v	=	Overburden stress, MPa
T	=	Temperature, ° C
T_{bh}	=	Horizontal well bottomhole temperature, ° C
$T(t,r,z,\theta)$	=	Temperature distribution in the system, ° C
T_f	=	Fluid temperature, ° C
$T_{f,th}$	=	Undisturbed formation temperature, ° C
T_g	=	Geothermal temperature, ° C
T_{inj}	=	Surface injecting fluid temperature, ° C
T_m	=	Temperature in tubing, ° C

t	=	Time, s
t_D	=	Dimensionless time
t^*	=	Dimensionless fracture surface exposure time
U	=	Internal energy per unit mass, J/Kg
U_o	=	Overall heat transfer coefficient, W/(m^2 ° C)
v	=	Fluid velocity, m/s
v_r	=	Radial fluid velocity, m/s
v_z	=	Vertical fluid velocity, m/s
w	=	Fracture width, m
w_D	=	Dimensionless fracture width
w_e	=	Fracture width change by net stress effect, m
w_p	=	Fracture width change by net pressure effect, m

Greek Nomenclature

α	=	Thermal diffusivity, m^2/s
α_l	=	Linear thermal expansion coefficient, 1/°C
ϕ	=	Formation porosity
η	=	Poroelastic coefficient
μ	=	Fluid viscosity, Pa.s
ρ	=	Fluid density, Kg/m^3
ν	=	Poisson ratio
$\sigma_{\min,corr}$	=	Minimum correspoinding horizontal stress, MPa

τ	=	Viscous force, N/m^2
$\psi(z)$	=	Geothermal temperature function, $^{\circ}C$